GAS EMISSIONS FROM LAKE KIVU

N.D. Fowkes* , D.P. Mason † and A.J. Hutchinson‡

Industry Representative

Denis Ndanguza

Study Group Participants

K. Anderson, O.F. Egbelowo, S. Hurwitz, J. Julyan, M. Khalique, B. Khomisa, R. Narain, J.M. Ngnotchouye, S. Oloniiju and N. Seeban

Abstract

Lake Kivu on the Rwanda-Congo border is one of three known lakes that have dangerous accumulations of methane and carbon dioxide trapped within their depths. There is concern that the gases could be spontaneously released leading to massive destruction and life loss, as has occurred in Cameroon in Lake Nyos in 1986 and Lake Monoun in 1984. Here we investigate some of the processes that cause the accumulation of gases that may lead to an eruption. We also examine power extraction issues.

1 Introduction

Lake Kivu is on the border between the Republic of Rwanda and the Democratic Republic of Congo and is one of three *killer lakes*, the others being Lake Nyos and Lake Monoun in Cameroon, see Figure 1. These lakes are very deep and heavily stratified with large quantities of methane and carbon dioxide trapped within the heavier lower layers. The spontaneous release of these gases at Lake Nyos in 1986 and at Lake

*Mathematics Department, University of Western Australia, Crawley, Australia *email: neville.fowkes@uwa.edu.au*

†School of Compter Science and Applied Mathematics, University of the Witwatersrand, Johannesburg, South Africa *email: david.mason@wits.ac.za*

‡School of Compter Science and Applied Mathematics, University of the Witwatersrand, Johannesburg, South Africa *email:hutchinson.ash@gmail.com*

Figure 1: Location of the killer lakes in Cameroon and Rwanda [1].

Monoun in 1984 caused massive destruction in the area and 1700 lives were lost, see Figure 2. In the case of Kivu, 300 km^3 of carbon dioxide and 55-60 km^3 of methane gas is trapped at depth in the lake, that is 300 times more gas than in Nyos before its eruption. An eruption at Kivu would be disastrous; there are two million people living in the area. In fact there is evidence of eruptions at Kivu in about 1000 year cycles and predictions based on observed accumulation rates (10-14% per year) suggest an eruption in the next 100-200 years, see Report [1].

Figure 2: Lake Nyos (1987): before and after the eruption [1].

The Study Group was asked to examine relevant scientific issues including those related to the safe extraction and use of methane for power production in the area.

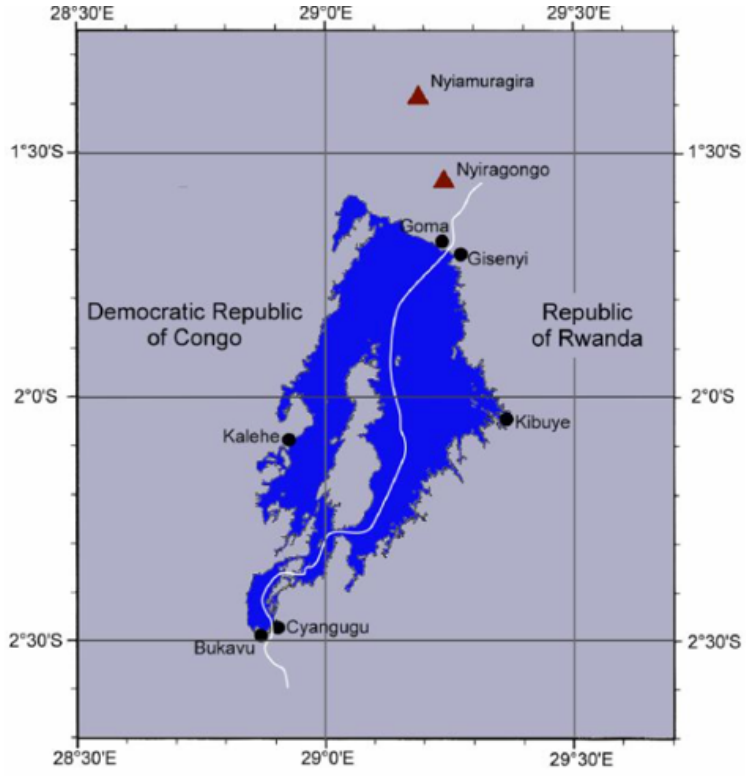

Figure 3: Lake Kivu plan [1].

There is a small (3.5 MW) test power station that has been operating since 2007. Earlier (July 2006) an expert committee produced an excellent Expert Committee Report on the Lake Stability [1] and much of the data collected in this report will be used to assist in the study to follow. Many of the results obtained in this article confirm those obtained by the committee and as such offer no new insights but at least provide confirmation. There are however new results that we think are useful.

Lake Kivu is a fresh water lake that is approximately 90 km long and 50 km at its widest and has a total surface area of about 2700 km^2, see Figure 3. The surface sits at a height of 1,500 m above sea level. The lake has a maximum depth of 474 m and a mean depth of 220 m, making it the world's eighteenth deepest lake by maximum depth and 9 th largest by mean depth. The total lake volume is about 550 km^3. The lake bed sits upon a rift valley that is slowly being pulled apart, causing volcanic activity in the area. Nearby is the volcano Nyiragongo, see Figure 4. Most of the gases of interest are likely to have this volcanic source. The world's tenth-largest island on a lake, Idjwi, lies in Lake Kivu, within the boundaries of Virunga National Park. Settlements on the lake's shore include Bukavu, Kabare, Kalehe, Sake and Goma in Congo, and Gisenyi,

Kibuye, and Cyangugu in Rwanda. There are about 2 million people in the area.

1.1 Geological and hydrological structure

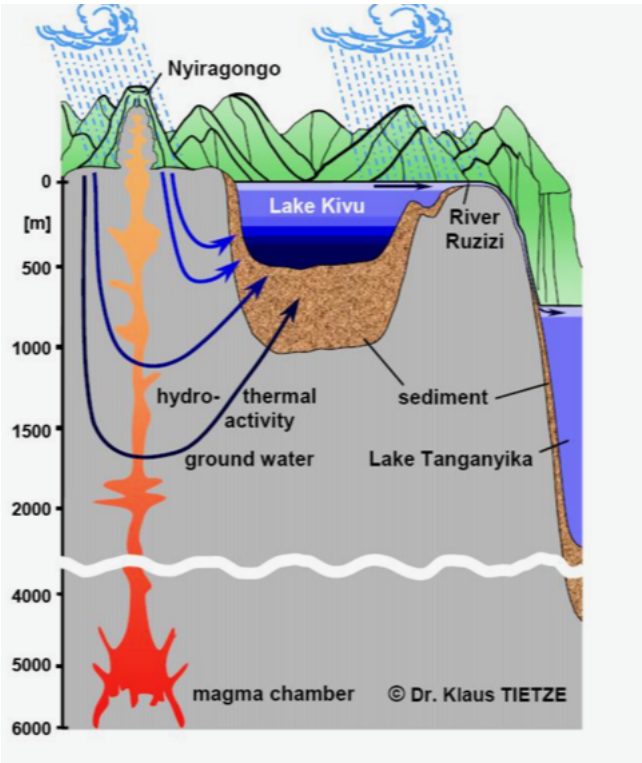

Figure 4: Lake Kivu: a section. Note that the lake is deep (500 m) and stratified as the shading indicates, see Figure 5. Nearby sits the volcano Nyiraongo which is the primary source of carbon dioxide. The methane derives from the biological degradation of organic matter near the bottom [1].

A simple schematic of the hydrological situation is shown in Figure 5. The lake is strongly stratified into layers separated by locations of rapid density changes: the thermocline is located at 60 m below the surface and there is a picnocline a further 200 m below the surface. Above the thermocline there is the biozone, so named because within this layer there is a plentiful supply of oxygen necessary for biological growth; surface stresses cause efficient mixing throughout this layer. This layer is fed primarily through run off from the surrounding ground and there is a through-flow via Lake Ruzizi into Lake Tanganyika. There are other more minor rivers feeding into and out of the lake.

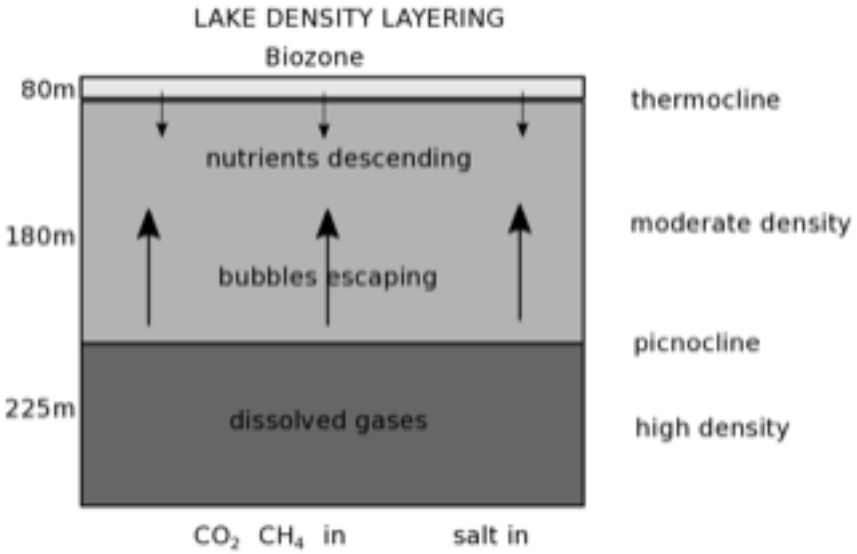

Figure 5: Schematic: density stratification in Lake Kivu. There are basically three layers separated by a thermocline at 80 m and a picnocline at 260 m [1].

Below the thermocline the density is significantly larger than within the biozone, and as a result there is little fluid motion and little interaction with the biozone. A further rapid increase in density occurs across the picnocline at 260 m, and it is below the picnocline that most of the volcanic gases are trapped. It would appear that groundwater passing close to the volcanic region carries the volcanic gases into the two lower layers. Also much of this groundwater passes through the very deep sedimentation layer below the lake, see Figure 4. This zone likely contains nutrients carried into the lake from above. The lowest density layer is estimated to contain 300 km^3 carbon dioxide and $55-65$ km^3 methane. The local stability of this stratified hydrological structure can be assessed by estimating the relative density gradient $\frac{\mathrm{d}\rho}{\mathrm{d}z}/\rho$ as a function of depth z; a locally high value of this index indicates that turbulent disruptions to the local density structure are unlikely. Looking at Figure 6 one can see that dynamic changes in the locations of the thermocline and picnocline are unlikely unless there is a dramatic geological event. It would appear that the borders of these zones are determined by overall hydrological issues and that changes to the depths of these zones are not likely to happen; models developed later assume this situation. A more detailed picture of the density structure is shown in Figure 7, and Figure 8 provides an estimate for the gas levels required for saturation in the lower layer; if such levels are exceeded the Lake will spontaneously 'boil'.

According to Schmid et al [4], there are three major risks that could potentially

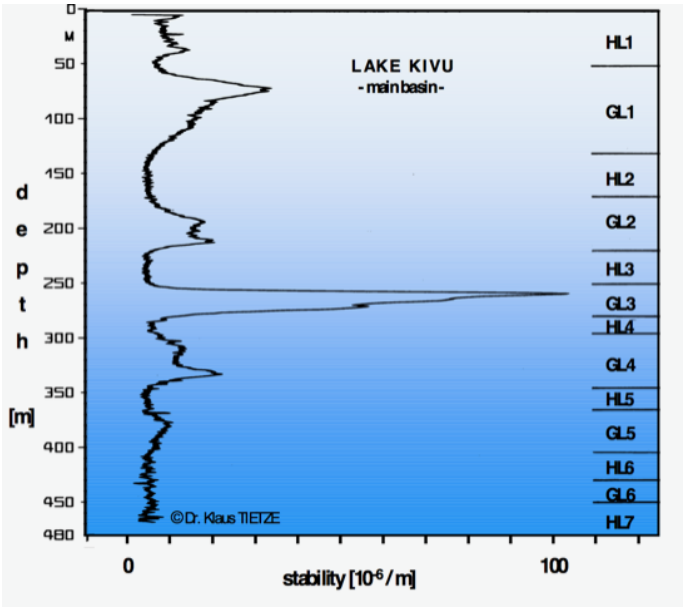

Figure 6: Stability: the bigger the relative density gradient the bigger the resistance to turbulent mixing. Note that this relative density gradient is large near the thermocline and the picnocline [1].

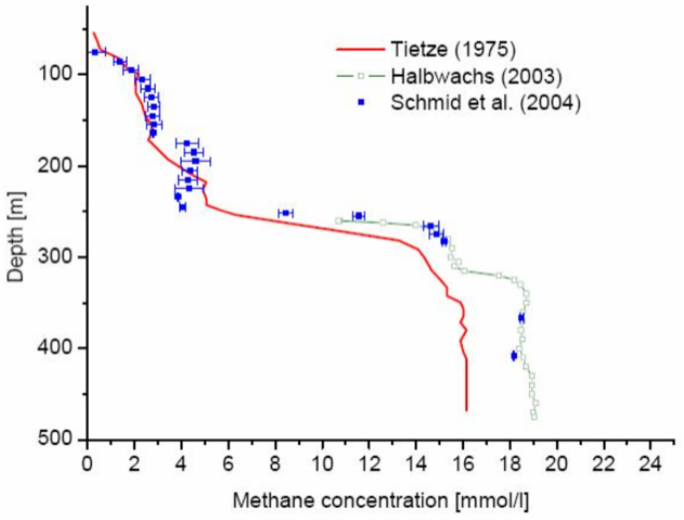

Figure 7: Methane concentration levels from 1975 to 2004, reproduced from the Lake Kivu gas extraction Report [1].

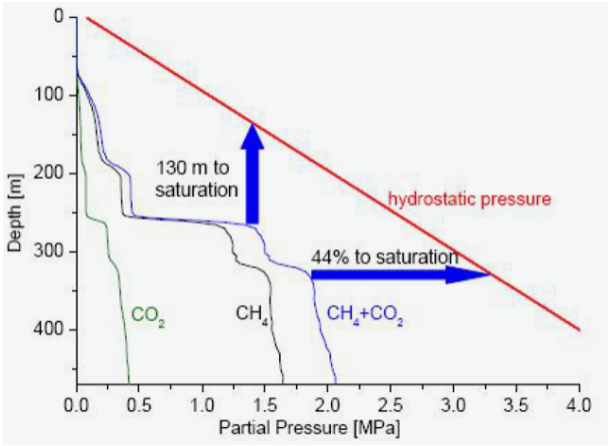

Figure 8: Estimated gas pressures based on 2003/4 data and perceived saturation risks [1]. If concentration levels reach beyond saturation (the red line) then an eruption will occur.

trigger a gas eruption:

- relatively small uplift of water by a strong internal wave
- a volcanic event could produce sufficient thermal energy that would lift water with high gas concentrations to a level where it is oversaturated and bubbles could form;
- a large amount of gas could be injected into the lake, for example by a gas release from the sediments triggered by intruding magma.

These risks have directed many of the investigations. As indicated most of the data above comes directly out of the Lake Kivu gas extraction Report [1] and this data will be used to examine certain issues in more depth.

In Section 2 factors related to the accumulation of gases and nutrients within the sublayers are investigated and associated stability issues are considered. Additionally the effect of the removal of gases (as in a power station) on the density structure are investigated. In Section 3 we examine gas solubility and bubble production issues and further examine the effect of an eruption on the release of gas from the lowest layer. Catastrophic release of trapped gases in the lower layer may occur if internal waves are generated within the stratified region and this is likely to happen if there is an earthquake or mud slide. The generation of such strong internal waves in discussed in Section 4. In Section 5 we use a simple chimney model to determine the gas and water flux that will result using the siphon system for power generation. Finally in Conclusions 6 we summarise our findings.

2 Gas accumulation and stability

Lake Kivu has a highly complex structure that is comprised of stratified layers. In this section, the lake is divided into four layers: The top layer, which refers to the biozone; a gradient layer at a depth of approximately 80m which protects the overlying biozone; another gradient layer at a depth of approximately 260m; and a bottom layer into which the gases are deposited [1]. The lower gradient layer acts as a barrier to the bottom layer where the gases are deposited which causes an accumulation of gases. Before discussing the various properties of the layers of Lake Kivu, it is important to understand the term 'lake stability'. If a less dense fluid lies on top of a denser fluid, there will be no movement and very little mixing. However, if a heavier fluid lies above a lighter fluid, mixing will take place. Lake stability refers to the situation where the density of the water increases with depth [1]. Variations of the key parameters with depth as obtained by Tietze [3] are displayed in Figure 9. The densities of the layers are dependent on the following properties [1]:

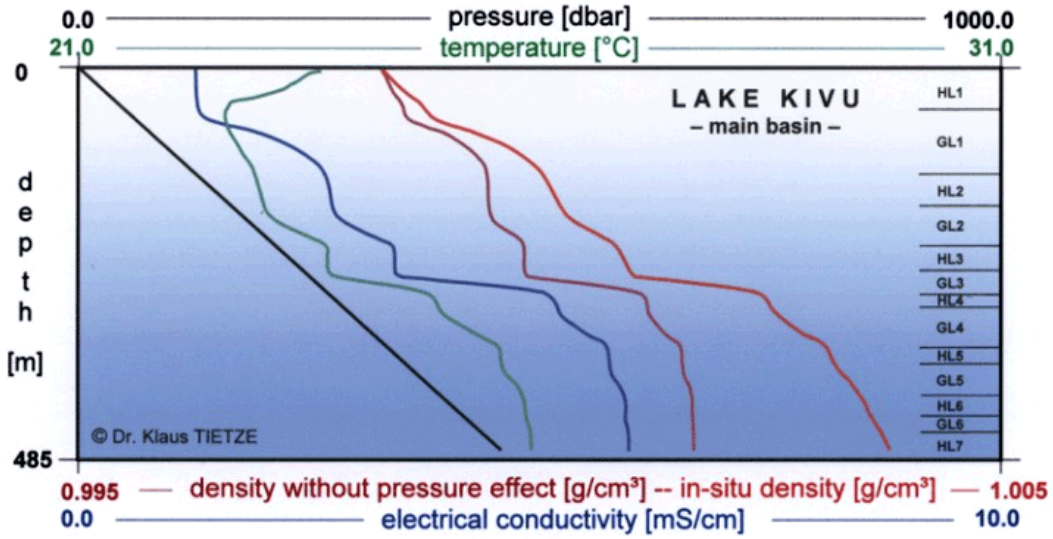

Figure 9: Variations of key parameters with depth in Lake Kivu (after [3]).

- Temperature - In most lakes, the temperature decreases with depth and therefore the density increases with depth resulting in lake stability. However, the situation in Lake Kivu is more complicated. Here the temperature starts to increase with depth below 80m. Lake Kivu remains stable because the effects of a decrease in density with depth due to temperature variations is compensated by the effect of the dissolved gases [4].

- Concentration of dissolved salts - Dissolved salts cause an increase in the density of the water. These salts settle at the bottom of the lake and therefore aid in lake stability. However, these salts are vital to living organisms in the biozone layer and although their transport out of the biozone layer helps maintain lake stability, it has a detrimental effect on the living organisms.

- Concentration of dissolved gases - Dissolved carbon dioxide increases the density of water. However, dissolved methane decreases the density of water. In the bottom layer, both methane and carbon dioxide are deposited. Accumulation of methane gas could disrupt lake stability.

- Pressure and depth - The density of the water in the lake increases with pressure and depth.

For our purposes it is convenient to divide Lake Kivu into four relatively distinct regions, see Figure 10:

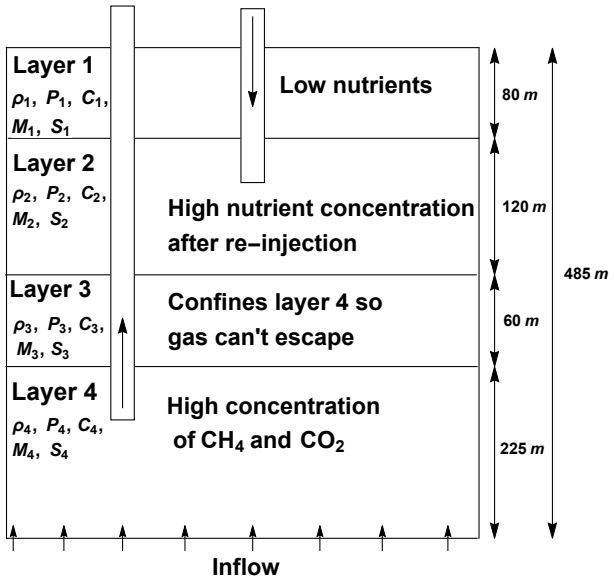

Figure 10: Stratified layers in the Lake

- Layer 1: The biozone layer or thermocline: An inflow of fresh water into the top layer supports life in the biozone. This region is oxygen rich. However, the nutrients sink through this layer to settle at the bottom of the lake, depriving living organisms of these essential nutrients. This means that this layer is not as good for life support as one would hope, see later [1]. Additionally, the continuous

bubbling of methane through this layer can be a threat to marine life as well as humans; swimmers have drowned because of asphyxiation.

- Layer 2: This layer is below the thermocline and thus is not stirred by surface winds.

- Layer 3: This gradient layer prevents the gases that accumulate in the bottom layer from being released. It essentially traps the carbon dioxide and methane.

- Layer 4: Carbon dioxide and methane are deposited into this layer. Because the layer above prevents the gases from escaping, the levels of these gases increase with time. Water from this layer is pumped out during the extraction process.

Equations describing the concentrations of salts, carbon dioxide and methane gas in each layer are formulated. The equations developed are based on the assumption that the depth of these layers is determined by 'external' hydrological factors and thus remain unchanged as gases accumulate in the various layers. The depth of the thermocline will vary seasonally but not by much, and fluxes of 'surface water' into and out of the lake will occur into this portion of the lake unless the density of these waters is large. The isopicnic location which separates the second layer from the third layer is likely to be determined by the hydrographical structure of the lake as well as groundwater flow. The time scale associated with such external forcing is likely to much greater than that associated with changes in gas concentration (100 years).

2.1 Concentration Equations

Both methane and carbon dioxide enter into layer 4 through groundwater. The extraction of water rich in methane, carbon dioxide and nutrients from the bottom layer and the re-entry of the processed water with a high nutrient content, but low carbon dioxide and methane gas concentrations, into the second layer is also incorporated into the model. The relevant conservation equations for these gases and the salts and nutrients are given by:

Methane

$$\begin{aligned}
\frac{\mathrm{d}M_4}{\mathrm{d}t} &= -\alpha_4(M_4 - M_3) + k_1 \ , \\
\frac{\mathrm{d}M_3}{\mathrm{d}t} &= -\alpha_3(M_3 - M_2) + \alpha_4(M_4 - M_3) \ , \\
\frac{\mathrm{d}M_2}{\mathrm{d}t} &= -\alpha_2(M_2 - M_1) + \alpha_3(M_3 - M_2) + I(t) \ , \\
\frac{\mathrm{d}M_1}{\mathrm{d}t} &= \ \ \alpha_2(M_2 - M_1) + \alpha_1(M_A - M_1) \ .
\end{aligned}$$

Here, M_i is the methane concentration in the various layers with $M_4 > M_3 > M_2 > M_1$, M_A is the methane concentration in the atmosphere and k_1 is the inflow rate kg/sec through groundwater. The term $I(t)$ represents the methane that is injected into layer 2 after the extraction process. Although it is likely that $I(t)$ can be neglected, for clarity it is included.

Carbon Dioxide

$$\begin{aligned}
\frac{\mathrm{d}C_4}{\mathrm{d}t} &= -\beta_4(C_4 - C_3) + k_2 \ , \\
\frac{\mathrm{d}C_3}{\mathrm{d}t} &= -\beta_3(C_3 - C_2) + \beta_4(C_4 - C_3) \ , \\
\frac{\mathrm{d}C_2}{\mathrm{d}t} &= -\beta_2(C_2 - C_1) + \beta_3(C_3 - C_2) \ , \\
\frac{\mathrm{d}C_1}{\mathrm{d}t} &= \ \ \beta_2(C_2 - C_1) + \beta_1(C_A - C_1) \ .
\end{aligned}$$

Here, C_i is the concentration of carbon dioxide in the i'th layer, with $C_4 > C_3 > C_2 > C_1$, C_A is the concentration of carbon dioxide in the atmosphere and k_2 is the inflow rate of carbon dioxide. When water is re-injected into layer 2 after the extraction process, it is assumed that all carbon dioxide has been removed.

Salts and Nutrients

$$\begin{aligned}
\frac{\mathrm{d}S_4}{\mathrm{d}t} &= -\gamma_4(S_4 - S_3) \ , \\
\frac{\mathrm{d}S_3}{\mathrm{d}t} &= \ \ \gamma_3(S_2 - S_3) + \gamma_4(S_4 - S_3) \ , \\
\frac{\mathrm{d}S_2}{\mathrm{d}t} &= -\gamma_2(S_2 - S_1) + k_3(t) - \gamma_3(S_2 - S_3) \ , \\
\frac{\mathrm{d}S_1}{\mathrm{d}t} &= \ \ \gamma_2(S_2 - S_1) \ .
\end{aligned}$$

Here, S_i is the concentration of salts and nutrients in the i'th layer, with $S_4 > S_2 > S_3 > S_1$. Nutrients that leave the biozone to settle into lower parts of the lake are re-introduced into the second layer after the extraction process as indicated by the term $k_3(t)$.

2.2 Density and temperature variations

The layers stratify because of density differences arising from factors such as temperature gradients, concentrations of dissolved salts and gases, pressure and depth. Lake stability is threatened by the accumulation of methane gas in the bottom layer which

decreases the overall density. Carbon dioxide has the opposite effect which increases the density. Empirical results give [4]:

$$\rho(T, S, C, M) = \rho(T)\left(1 + \beta_s S + \beta_c C + \beta_m M\right),$$

where

$$\beta_s = 0.75 \times 10^{-3} kg.g^{-1},$$
$$\beta_c = 0.284 \times 10^{-3} kg.g^{-1},$$
$$\beta_m = -1.25 \times 10^{-3} kg.g^{-1},$$
$$\rho(T) = \frac{\rho_w}{0.002 + \Delta T + 1},$$

and ρ_w is the density of water at standard temperature and pressure.

2.3 Concentration profiles through the Lake

Based on the above model equations a number of simulations were carried out, a sample of which are displayed in Figures 11, 12 and 13. It should be noted that the concentrations of methane, carbon dioxide and salts affect the density of the layers in the lake. Lake stability is not obtained in many cases.

The simulation shown in Figure 11 represents an ideal situation where the concentration of salts and nutrients increases in the upper layer and lake stability is maintained. These results can be achieved by careful management of the extraction and re-injection process. In Figures 12 and 13, lake stability is not maintained. In Figure 12, the deepest two layers remain stable but the upper two layers do not. In Figure 13 the salt concentration increases in the upper layer but the lower levels are unstable. Improper management of the extraction process or a lack of intervention would likely cause this result.

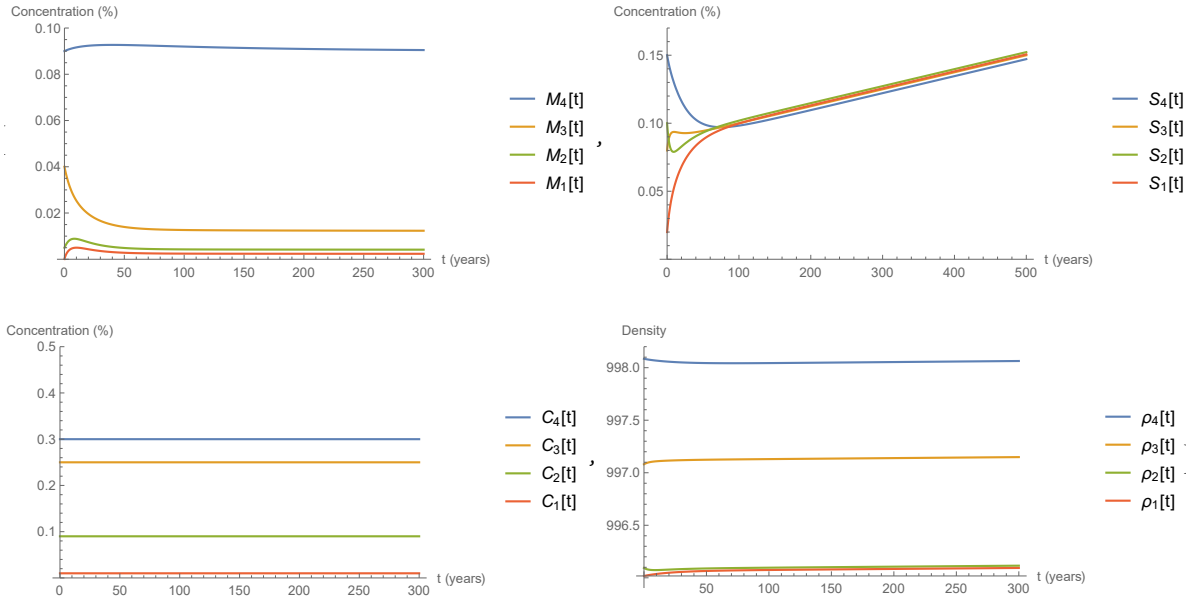

Figure 11: Concentrations of methane M_i, salts S_i, carbon dioxide C_i and the density of each layer in Lake Kivu. In this scenario, lake stability is maintained and the salt concentration is successfully increased in the biozone.

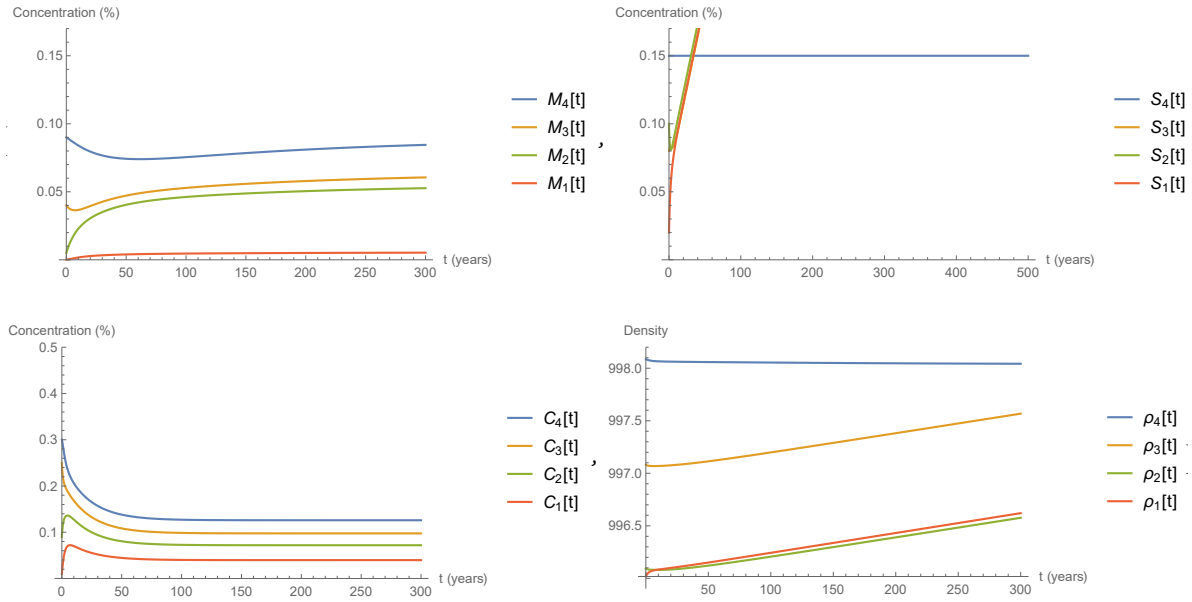

Figure 12: Concentrations of methane M_i, salts S_i, carbon dioxide C_i and the density of each layer in Lake Kivu. In this scenario, the methane concentration increased in the bottom layer. Lake stability is not maintained.

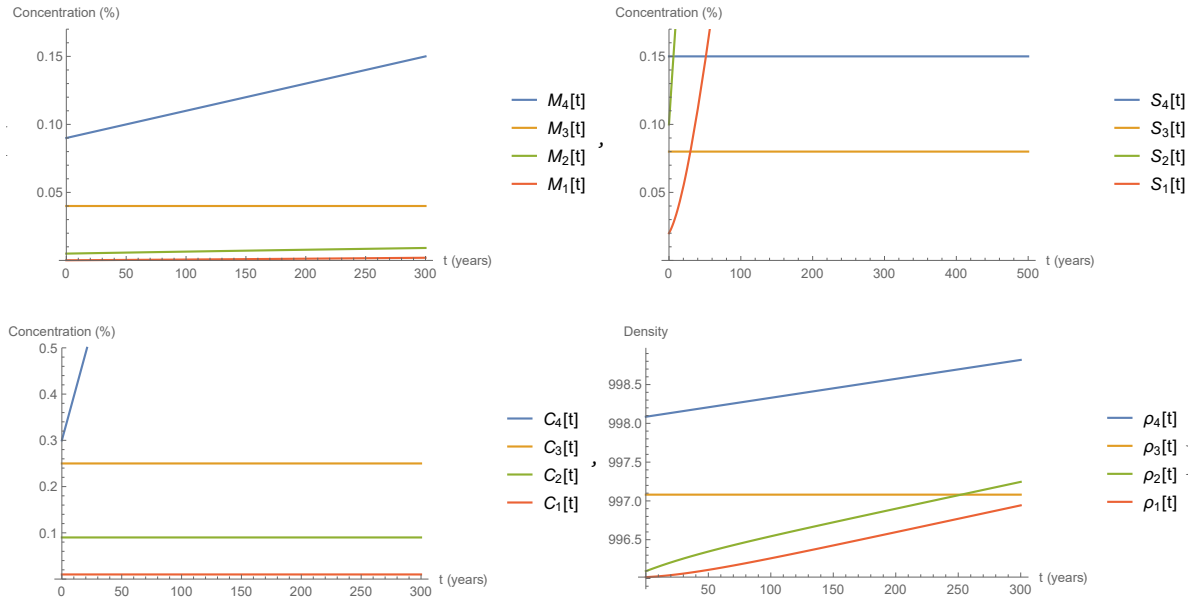

Figure 13: Concentrations of methane M_i, salts S_i, carbon dioxide C_i and the density of each layer in Lake Kivu. In this scenario, the methane and carbon dioxide concentrations increase in the bottom layer. Lake stability is not maintained.

2.4 Methane levels and extraction models

In the absence of extraction, methane levels are observed to increase linearly in time, see Figure 7, evidently described by

$$\frac{\mathrm{d}M}{\mathrm{d}t} = \kappa \,,$$

where κ is the inflow rate of methane from underground and $M(t)$ is the total volume of methane, mainly at levels 3 and 4. If one assumes a uniform extraction rate from power plants using a siphon process, see Figure 15, then

$$\frac{\mathrm{d}M}{\mathrm{d}t} = \kappa - C_T$$

describes the process, where C_T is the total extraction rate from all processing plants.

A more realistic model would be

$$\frac{\mathrm{d}M}{\mathrm{d}t} = \kappa - C_T M \,,$$

however, data is provided in such a way that the extraction rate is constant, regardless of the volume of methane in the lake. We have data from 2004 relating the methane volume in 2004 to 1975, and based on this data we find $\kappa = 2.47 \times 10^{-10}$ Mm^3 yr^{-1}; according to literature, the value of κ ranges from 1.71×10^{-10} Mm^3 yr^{-1} to 2.5×10^{-10}Mm^{3}yr^{-1}. Using the results for κ we have plotted expected methane levels in the lake, see Figure 14. These results are broadly consistent with those given in the report [1], suggesting they used the same or equivalent assumptions.

2.5 Power plant extraction

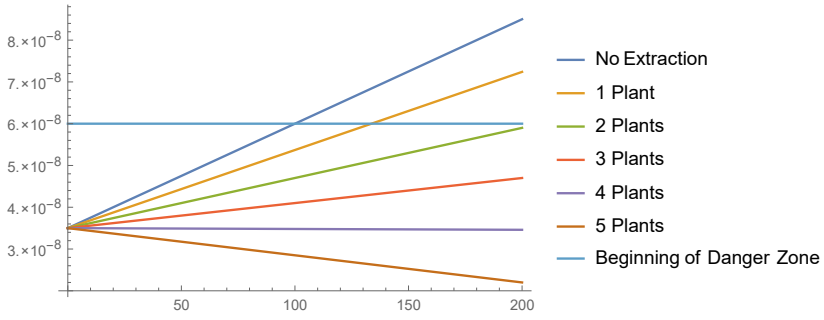

Figure 14: Methane levels in the presence of power stations.

The extraction rate of the KP1 plant is 6.29×10^{-11}Mm^{3}yr^{-1}. Based on this figure we have calculated the effect of a number of plants of this size on levels of methane

in the lake. The results are displayed in Figure 14, where we plot concentration levels in the lake as a function of years from the present. The horizontal line corresponds to saturated levels in the lake. We can see from this figure that saturated conditions are expected 100 years from now in the absence of extraction, and if five plants are used then concentration levels in the lake are predicted to remain unchanged.

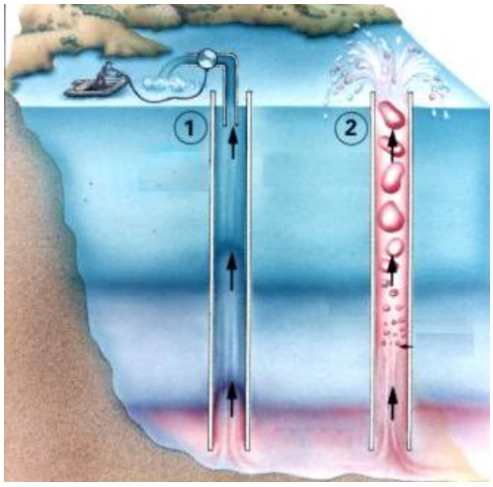

Figure 15: Siphoning off gases, and a power plant using a siphon [1].

3 Bubble formation and movement

Carbon dioxide and methane gases are both soluble in water and in this aqueous form are released into the bottom layer of Lake Kivu to accumulate over time, see Figure 8. Until supersaturation levels are reached these gases will remain in aqueous form and will not bubble to the surface of the lake, and so do not pose an immediate risk. As indicated earlier and as displayed in Figure 8, present saturation levels in this lower layer are at most 44% with this level being reached at the top of the lower stratified layer at roughly 225 m depth. Recorded accumulation rates suggest saturation levels will be reached in about 100 years if the supply rate remains at present levels. This assumes, however, that there are no significant eruptions. The saturation concentration level increases with pressure so that if fluid particles carrying gas are carried upwards then under the associated reduced pressure conditions gasification may occur with the gases then bubbling to the surface. At the present time particles would need to move vertically a distance of 130 m in order for gasification to occur, see Figure 8. Such a vertical movement of fluid particles is unlikely unless there is a catastrophic volcanic eruption. However as concentration levels increase more moderate eruptions

may results in internal waves of sufficient magnitude to cause gasification. We examine this situation here and in the next section.

We first describe the processes of bubble formation and movement and in the followup section we will discuss internal wave generation in the Lake Kivu context. It should be noted that carbon dioxide has a much larger solubility than methane (a factor of 5) and so is less likely to form bubbles than methane, so, although carbon dioxide volumes in the lake are five times greater than methane volumes, gas release is primarily a methane phenomenon for Lake Kivu. It can be seen in Figure 8 that in the Lake Kivu case that methane contributes 80% to the partial pressure with carbon dioxide just 20%. With this in mind our discussions below will be concerned with the vaporization of a single gas which we will think of as being methane.

3.1 Nucleation and bubble growth

Consider a closed vessel containing water with a single absorbed gas (methane) and with a headspace above the water also containing a small amount of the gas. An evaporative/condensation exchange of the gas occurs between the two phases until thermodynamic equilibrium is attained. Henry's Law relates the concentration of the absorbed gas in the water c_l to the partial pressure of the gas p in the headspace once thermodynamic equilibrium is reached:

$$c_l = H(T)p, \text{ or equivalently } p = k_H(T)c_l. \tag{3.1}$$

Aside: Henry's constant H varies with temperature (more gas is released by the liquid phase at higher temperatures) and the van't Hoff equation

$$k_H(T) = k_H^0 \exp\left[-C\left(\frac{1}{T} - \frac{1}{T_0}\right)\right] \tag{3.2}$$

is used to describe the variation with C fitted to experimental results. Here T_0 refers to the standard state temperature 298.15 K. For methane k_H=56.9 atmos/(mol/litre) or 5.69 MPa/(mol/litre) at $T = 25^\circ$ C). In the Lake Kivu context pressure effects dominate temperature effects so to first order the temperature effects can be ignored.

If the vessel is open then no such equilibrium is reached *except* within a diffusive boundary layer close to the surface. Outside this boundary layer the gas will disperse into the far environment in response to external (conductive and convective) exchanges.

Whilst Henry's law also applies to a bubble in contact with a liquid one needs to account for the additional pressure drop across the surface of the bubble due to surface tension described by Laplace's Law

$$p_b = p_l + \frac{2\sigma}{R}; \tag{3.3}$$

here p_l is the pressure in the liquid just outside the bubble, p_b is the pressure just inside the bubble surface, R is the bubble radius and σ is water/air surface tension. Thus the exchange of gas molecules across the bubble surface will balance and we will have thermodynamic equilibrium realised when

$$c_l = H(T)p_b \equiv c_b = H(T)(p_l + 2\sigma/R), \tag{3.4}$$

where we have identified c_b as being the equivalent bubble 'concentration' which is normally defined in terms of the associated partial pressure p_b in the bubble.

Thus, using (3.4) and solving for R we see that equilibrium will only be realised for a bubble with radius given by the critical value

$$R_c = \frac{2\sigma}{(c_l/H - p_l)}. \tag{3.5}$$

However this equilibrium is unstable. For if $R < R_c$ then $c_l < c_b$, so gas is expelled from the bubble and it shrinks, whereas if $R > R_c$ then $c_b > c_l$ and the bubble grows. Thus bubbles with radius less than the critical radius will disappear and won't normally be created or seen, whereas those with radius greater than this critical value will continue growing. The critical radius result is often expressed in terms of the supersaturation ratio

$$S = \frac{c_l}{Hp_l} - 1,$$

in terms of which

$$R_c = \frac{2\sigma}{p_l S}; \tag{3.6}$$

thus supersaturated conditions are required ($S > 0$) for bubble growth and, even under supersaturation conditions, the bubbles need to be large enough to survive and grow. Note that the bubble size for growth varies inversely with the supersaturation level S, so the higher the saturation level the greater the probability of bubble formation. The critical radius for methane bubbles at atmospheric pressure is $R_c = 1.44$ μm for $S = 1$ which is very small. At the picnocline at a depth of 225 m the hydrostatic pressure is about 20 p_a so the critical radius is much smaller.

The effect of surface tension is thus dramatic and perhaps can be best explained in terms of the energy requirements for bubble formation. Surface tension tends to contract the surface so that there is an energy barrier that needs to be overcome before bubbles can be formed even when thermodynamically conditions prevail i.e. $S > 0$. Note especially that the surface tension effect is *very large* for small radius bubbles, so that bubbles cannot grow from an initial radius $R = 0$; as shown above the bubble's radius must in fact be greater than R_c for it to grow. This explains why *homogeneous nucleation* (that is growth in the body of the fluid) will not normally occur; the probability of enough gas molecules in the liquid finding themselves at the same location to form a critical radius bubble is very small. However gas can

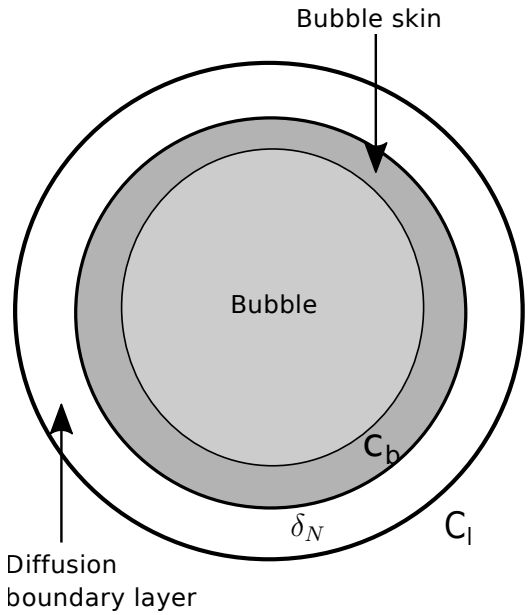

Figure 16: Gas transfer across the surface of a bubble. There is a concentration difference between the dissolved gas in the liquid bulk and the dissolved gas concentration $c_b = Hp_b$ in the bubble skin given by $\Delta c = c_l - c_b$. The concentration falls from c_l to c_b over a diffusion boundary of thickness δ_N.

accumulate, and bubbles form, on a sufficiently large particle within the liquid or indentation in the containing vessel; these particles/indentations are called nucleation sites and the process is referred to as *heterogeneous nucleation*. In the Lake Kivu case there will be many nucleation sites (dust etc.) so that heterogenous nucleation will result in bubble release under supersaturation conditions.

Bubbles will move vertically in the liquid because of buoyancy and additionally may be swept along in any background flow. Because of this movement the fluid particles surrounding the bubble will be continuously exchanged so that the bubbles will be surrounded by liquid with absorbed gas concentration c_l, that is the undisturbed concentration in the water locally. Under such circumstances the concentration difference driving the evaporative exchange is given by $\Delta c = c_l - c_b \equiv c_l - Hp_b$ and the associated flux will be $k\Delta c$, where k is the mass transfer coefficient. This mass transfer coefficient can be estimated by assuming that gas transfers by diffusion across a skin of thickness δ_N, see Figure 16. Based on a simple model one can estimate δ_N in terms of the flow variables and this gives

$$\kappa = k/\rho_b = \left(\frac{\mathrm{D}}{2}\right)^{2/3} \left(\frac{\rho_l g}{9\mu_l}\right)^{1/3} /\rho_b,$$

see ([9]), where D is the diffusion coefficient for methane in water. With D= 1.88×10^{-9} m ^{2}/s [10], ρ_b= 1.22 kg/m^3, this gives $\kappa = 1.0\ \mu$ m/sec. Mass conservation for the bubble gives

$$\frac{\mathrm{d}}{\mathrm{d}t}\left(\frac{4}{3}\pi R^3\rho_b\right) = k(4\pi R^2)\Delta c \ = \ k(4\pi R^2)\left[c_l - H(p_l + 2\sigma/R)\right],$$

which, using (3.3), (3.4) and (3.5), can be written in the form

$$\frac{\mathrm{d}}{\mathrm{d}t}\left(\rho_b R^3\right) = kR^2\left[\delta c_d + 6\sigma H\left(\frac{1}{R_c} - \frac{1}{R}\right)\right], \text{ where } \delta c_d = c_l - c_l^{eql}(p_l). \tag{3.7}$$

Here $c_l^{eql}(p_l)$ is the liquid concentration corresponding to the bubble equilibrium concentration at liquid pressure p_l and at the associated bubble radius $R_c(p_l)$. In this form we have 'separated out' the various processes causing bubble growth or collapse: gas transfer across the bubble surface, surface tension driven adjustments, and pressure induced adiabatic expansion or contraction. Thus if a bubble of radius R_0 is introduced into the solution there will be a quick surface tension adjustment (exponentially with time scale $R_c/(2H\sigma)$) which will collapse the bubble if $R < R_c$, or will expand the bubble if $R > R_c$. If $R_0 > R_c$ the bubble will first quickly expand and achieve mechanical equilibrium and then surface tension effects will become relatively small so that gas transfer effects then will dominate with the time scale of growth being $(\rho_b R_0)/(k\delta c)$. If there are significant changes in the pressure p_l then there will be associated bubble radius adjustments.

In the Lake Kivu situation there will be significant changes in the hydrostatic pressure acting on the bubble as it moves from its initial location z above the bottom of the lake to the surface at $z = h$ at pressure p_a described by

$$p_l(z) = p_a + \rho_l g(h - z).$$

This will produce a change in density of the bubble described by the perfect gas law

$$p_l(z) = \rho_b(z)RT(z)\ ,$$

which gives approximately

$$\frac{p_l(z)}{p_a} = \frac{\rho_b(z)}{\rho_a}, \tag{3.8}$$

where we have ignored changes in (absolute) temperature in the lake, being relatively small. Thus the bubble gas density will vary with depth according to

$$\rho_b(z) = \rho_a\left(1 + \frac{\rho_l g(h - z)}{p_a}\right). \tag{3.9}$$

At the picnocline (a depth of 225 m) the hydrostatic pressure is 2.1 MPa, which is 21 times the pressure at the surface of the lake, so that the density of bubble gas at the picnocline is 21 times of its value at the lake's surface. Thus there will be a large change in bubble size ($(\rho_z/\rho_a)^{1/3} = 2.75$) as it travels from this depth to the surface just due to (adiabatic) pressure adjustments.

3.2 Bubble movement

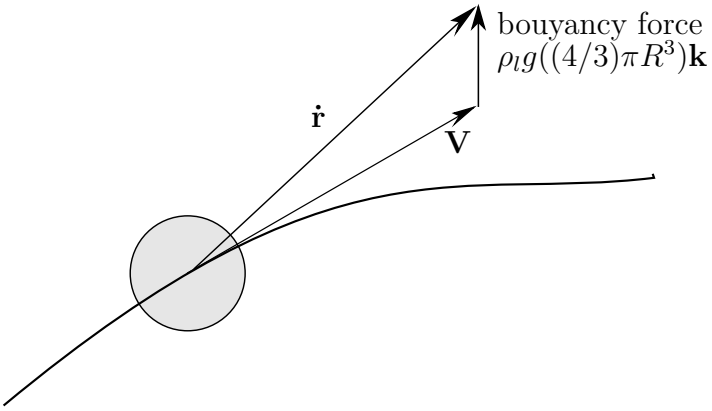

Figure 17: Bubble moving in a convection flow $\mathbf{V}$. The buoyancy force acts to deflect the path away from the flow.

Assuming the bubble, with effective zero mass, is moving with velocity $\dot{\mathbf{r}}$ in a prescribed flow field $\mathbf{V}$, then under quasi-steady conditions we have a balance between the Stokes drag acting on the bubble and the buoyancy force giving

$$(\mathbf{V} - \dot{\mathbf{r}})\alpha\pi R\mu_l + \rho_l \left(\frac{4}{3}\pi R^3\right) g\rho_l \mathbf{k} = \mathbf{0},$$

where μ_l, ρ_l are the dynamic viscosity and density of the liquid and the drag coefficient α lies in the range $4 < \alpha < 6$ for the bubbles depending on the absence/presence of surface-active impurities in the water (Batchelor[9]) so that we obtain

$$(\mathbf{r}\dot{\mathbf{t}}\mathbf{r} - \mathbf{V}) = \frac{4}{3\alpha}\frac{R^2 g\rho_l}{\mu_l}\mathbf{k}; \tag{3.10}$$

the buoyancy force causes the bubble to drift vertically away from the flow field, see Figure 3.2. Taking $\alpha = 6$ we obtain a drift velocity of 0.27 cm/s for a 5×10^{-5} m radius bubble ($\mu = 2 \times 10^{-3}$ Pa s, $\rho_l = 10^3$ kg /m^3) and this increases (rapidly) by a factor of 100 to 27 cm/s for a 5×10^{-4} m radius bubble; small bubbles move with the flow whilst bigger bubbles quickly escape the flow.

The coupled equations (3.7, 3.9, 3.10), together with initial conditions on bubble radius and depth, determine the motion and growth of individual bubbles in a prescribed flow field, hydrostatic pressure and gas concentration c_l environment.

In the Lake Kivu context considerable simplifications are possible. We are especially concerned with bubble growth and movement in the neighbourhood (say 10 m) of the pinocline located at 225 m where saturated conditions will be first reached; bubbles leaving this zone will expand by a factor of about 2.7 due to adiabatic expansion and rapidly accelerate to the lake surface with some additional gas transfer depending on concentration levels in the lake. Such details can be easily computed using the defining equations and will not be addressed here; our concern here is with what happens near the isopicnic (say within 10 m).

With the above in mind in the pinocline zone we can replace the bubble density ρ_h by its local value of $\rho_h = 21\rho_a$, and this leads to the simple result

$$\frac{\mathrm{d}R}{\mathrm{d}t} = \frac{k}{\rho_h}\Delta c \tag{3.11}$$

for bubble growth; density effects decouple. If we further ignore the initial surface tension induced changes then $\Delta c = \delta c_d$ so that, with a fixed supersaturation ratio, there will be a linear growth in bubble radius with time given by

$$\frac{\mathrm{d}R}{\mathrm{d}t} = \frac{k}{\rho_h}\delta c, \text{ so that } R(t) = (\frac{k}{\rho_b}\delta c)t + R_0, \tag{3.12}$$

with the (radius doubling) time scale of order $\rho_b R_0/(k\delta c)$. With a methane concentration of $\delta c_d = 1.1$ m^3/m^3 of water this give 44 secs for evaporative induce radius doubling. The associated drift in velocity from the background flow field is quadratic in bubble radius and thus quartic in time as seen from (3.10). Of course once the bubble escapes the picnocline zone there will be a further large change in bubble radius due to hydrostatic pressure changes and this in turn will induce a much accelerated motion.

4 Internal waves

It should be noted that the effect of surface winds on the lake are only seen in the upper 60 m so that the lower depths of the lake containing the absorbed gases will be unaffected. However geological eruptions can change the size and shape of the lake either directly by moving the walls or changing the depth or by causing underwater mud slides. Also lava may flow into the lake and an explosion could result. The situation is entirely analogous to a tsunami on the ocean; it is the vertical displacement of the water of the lake that provides the potential energy for the generated waves. The eruption may be 'instantaneous' or the vibration may be sustained as in an earthquake. The effect of this shape change will be to generate an internal wave on the interface between the higher density bottom layer and the lower density upper layers. Of course this movement will be transmitted to the upper stratified layers so what will be seen

will be a wave propagating backwards and forwards and around the island of the lake involving all layers. The energy of these waves will be slowly dissipated mainly through shoreline breaking. From our point of view it is the effect of such waves on the release of gases from the lower layers that is important. The fluctuations in wave height of the lake tsunami result in decreased (and also increased) hydrostatic pressures experienced by supersaturated fluid particles in the lower zone bubbles and this will cause bubbles to come out of solution as described in Section 3. Generally long waves will be generated by eruptions and (natural standing modes) seiching modes will be generated, and these modes are the most destructive for the gas release point of view. The lake is deep but nevertheless its depth is relatively small compared with its length and width so that long wave approximations are appropriate. Also small amplitude theory is appropriate; the amplitude of the waves will normally be very small compared with the depth.

We combine the three upper layers in Lake Kivu to form one uniform layer and analyse the properties of the internal waves on the interface between the lowest layer in the lake and the upper layer. This interface is called the picnocline. A diagram of Lake Kivu is presented in Figure 18. Both fluids are incompressible and inviscid. The flows are irrotational and are formulated in terms of velocity potentials. The long wavelength and small amplitude approximations are made. In Appendix A the problem is formulated mathematically and solved. In this section the results are analysed physically.

The concentrations of carbon dioxide and methane in the bottom layer of the lake could slowly increase until the sum of their partial pressures would tend to the local hydrostatic pressure. A sufficiently strong internal wave at the interface could lift the fluid a relatively small amount to a level where it is over-saturated and gas bubbles could form and rise due to buoyancy, thus triggering a gas eruption. We will obtain estimates for the phase velocity, period and pressure change for the internal wave and the wave induced on the lake surface. The orbit of a fluid particle in the lower layer due to the internal wave on the interface will also be studied.

Consider first the speed of the internal wave,

$$c = \frac{\omega}{k} = \pm \left[\frac{g}{2} \left(h_1 + h_2 \pm \left[(h_1 + h_2)^2 - \frac{4(\rho_1 - \rho_2)}{\rho_1} \, h_1 \, h_2 \right]^{1/2} \right) \right]^{1/2}, \tag{4.1}$$

which can be written equivalently as

$$c = \frac{\omega}{k} = \pm \left[\frac{g}{2} \left(h_1 + h_2 \pm \left[(h_1 - h_2)^2 + 4\frac{\rho_2}{\rho_1} \, h_1 \, h_2 \right]^{1/2} \right) \right]^{1/2}. \tag{4.2}$$

Equations (4.1) and (4.2) are derived in Appendix A as (A.64) and (A.65). There are two waves, the fast speed wave which we will refer to simply as the fast wave,

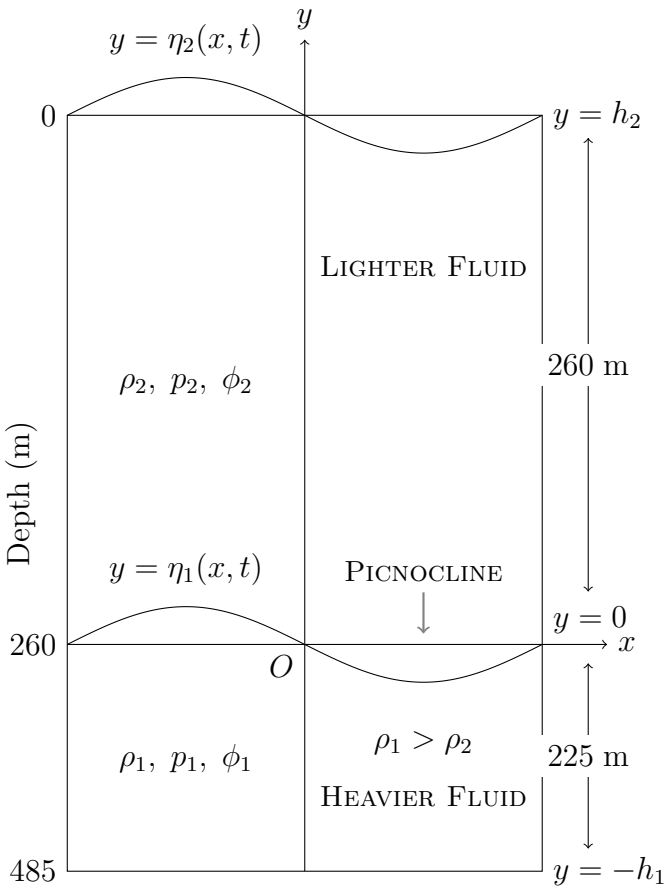

Figure 18: Diagram of Lake Kivu showing the coordinate system and an internal wave on the interface separating the denser lower layer from the less dense upper layer. The internal wave induces a wave on the lake surface.

with speed

$$c_+ = \frac{\omega}{k} = \pm\left[\frac{g}{2}\left(h_1 + h_2 + \left[(h_1+h_2)^2 - \frac{4(\rho_1-\rho_2)}{\rho_1}\, h_1 h_2\right]^{1/2}\right)\right]^{1/2}. \tag{4.3}$$

or equivalently

$$c_+ = \frac{\omega}{k} = \pm\left[\frac{g}{2}\left(h_1 + h_2 + \left[(h_1-h_2)^2 + 4\frac{\rho_2}{\rho_1}\, h_1 h_2\right]^{1/2}\right)\right]^{1/2} \tag{4.4}$$

and the slow speed wave or slow wave with speed

$$c_- = \frac{\omega}{k} = \pm \left[\frac{g}{2} \left(h_1 + h_2 - \left[(h_1+h_2)^2 - \frac{4(\rho_1-\rho_2)}{\rho_1}\, h_1 h_2 \right]^{1/2} \right) \right]^{1/2} \tag{4.5}$$

or equivalently

$$c_- = \frac{\omega}{k} = \pm \left[\frac{g}{2} \left(h_1 + h_2 - \left[(h_1-h_2)^2 + 4\frac{\rho_2}{\rho_1}\, h_1 h_2 \right]^{1/2} \right) \right]^{1/2} . \tag{4.6}$$

Since both the fast and slow waves travel in both directions standing waves can be generated.

We see from (4.4) that the fast wave is always stable even when $\rho_2 > \rho_1$ and the upper fluid is the heavier fluid. From (4.6) the slow wave is unstable if

$$\left[(h_1-h_2)^2 + 4\frac{\rho_2}{\rho_1}\, h_1 h_2 \right]^{1/2} > h_1 + h_2 \, , \tag{4.7}$$

that is if

$$\rho_2 > \rho_1 \, . \tag{4.8}$$

The slow wave is unstable if the density of the upper fluid is greater than that of the lower fluid which is the Rayleigh-Taylor instability.

Consider now approximate expressions for the wave speeds. From (4.3) and (4.5),

$$c_\pm = \frac{\omega}{k} = \pm \left[\frac{g}{2}\, (h_1+h_2) \right]^{1/2} \left[1 \pm \left(1 - \frac{4(\rho_1-\rho_2)}{\rho_1}\, \frac{h_1 h_2}{(h_1+h_2)^2} \right)^{1/2} \right]^{1/2} . \tag{4.9}$$

We expand $c_\pm$ for small values of δ where

$$\delta = \frac{4(\rho_1-\rho_2)}{\rho_1}\, \frac{h_1 h_2}{(h_1+h_2)^2} \, . \tag{4.10}$$

An estimate for δ is made when numerical values are substituted later. Neglecting terms of order δ^2, (4.9) gives

$$c_+ = \frac{\omega}{k} = \pm \big[g(h_1+h_2) \big]^{1/2} \left(1 - \frac{(\rho_1-\rho_2)}{2\rho_1}\, \frac{h_1 h_2}{(h_1+h_2)^2} \right) , \tag{4.11}$$

$$c_- = \frac{\omega}{k} = \pm \left[g \frac{(\rho_1-\rho_2)}{\rho_1}\, \frac{h_1 h_2}{(h_1+h_2)^2} \right]^{1/2} . \tag{4.12}$$

The fast speed c_+ is primarily dependent on the total depth of the lake while the slow speed c_- is strongly dependent on the difference in density across the picnocline.

The phase speed does not depend on wavelength. The internal waves are therefore non-dispersive.

The periods of the fast and slow waves are

$$T_+ = \frac{\lambda}{c_+} = \frac{\lambda}{\left[g(h_1+h_2)\right]^{1/2}} \left[1 + \frac{(\rho_1-\rho_2)}{2\rho_1} \frac{h_1 h_2}{(h_1+h_2)^2}\right] , \tag{4.13}$$

$$T_- = \frac{\lambda}{c_-} = \lambda \left[\frac{\rho_1(h_1+h_2)}{g(\rho_1-\rho_2)h_1h_2}\right]^{1/2} , \tag{4.14}$$

where λ is the wavelength. The fast wave is the high frequency wave while the slow wave is the low frequency wave. In order to estimate values for the wave speeds and the periods of the fast and slow waves we use

$$h_1 = 225 \text{ m} , \qquad h_2 = 260 \text{ m} ,$$

$$\rho_1 = 1001 \text{ kg m}^{-3} , \qquad \rho_2 = 1000 \text{ kg m}^{-3} , \qquad \lambda = 50 \times 10^3 \text{ m} \tag{4.15}$$

The estimates for the density are taken from the paper by Schmid et al [4] and do not include the effect of the pressure on the density. The maximum length of the lake is 89 km and the maximum width is 48 km. We therefore took for the wavelength 50 km. This gives from (4.10),

$$\delta = 9.94 \times 10^{-4} \ll 1 \tag{4.16}$$

and the approximation that terms $\mathrm{O}(\delta^2)$ can be neglected is justified. Also,

$$c_+ = 68.97 \,\text{ms}^{-1} , \qquad c_- = 1.09 \,\text{ms}^{-1} . \tag{4.17}$$

The spread of the fast wave is about 63 times greater than that of the slow wave. The periods of the fast and slow waves are

$$T_+ = 12.08 \,\text{mins} , \qquad T_- = 12.78 \,\text{hrs} . \tag{4.18}$$

The longer period of the slow wave gives more time for bubbles to be generated within the moving fluid and more time for the gases to escape from the interface. The slow waves correspond to lower frequency longer period waves and will be more strongly generated by low frequency geological vibrations and by secondary shocks several hours after a seismic event. These estimates of physical quantities depend strongly on the estimate for the density difference across the interface.

The internal wave at the interface is the real part of

$$\eta_1 (x,t) = \eta_{10} \exp \left[i(kx - \omega t)\right] . \tag{4.19}$$

For the fast wave for all positive values of ρ_1 and ρ_2 and for the slow wave with $\rho_1 > \rho_2$ the real part of (4.19) is

$$\eta_1(x,t) = \eta_{10}\ \cos\left[k(x - c_\pm t)\right] \tag{4.20}$$

where $c_\pm$ is given by (4.9) and in expanded form by (4.11) and (4.12). When $\rho_2 > \rho_1$ the slow wave is unstable and the real part of (4.19) is

$$\eta_1(x,t) = \eta_{10} \exp(\pm\beta t)\ \cos(kx) \tag{4.21}$$

where

$$\beta = k\left[\frac{g}{2}\ (h_1+h_2)\right]^{1/2}\left[\left(1 + \frac{4(\rho_2-\rho_1)}{\rho_1}\ \frac{h_1h_2}{(h_1+h_2)^2}\right)^{1/2} - 1\right]^{1/2}\ , \tag{4.22}$$

or neglecting terms of order δ^2,

$$\beta = k\left[g\frac{(\rho_2-\rho_1)}{\rho_1}\ \frac{h_1h_2}{(h_1+h_2)}\right]^{1/2}\ . \tag{4.23}$$

Dissolved salt and carbon dioxide increase the density, ρ_1, and stabilise the lower layer while dissolved methane decreases the water density and destabilises the lower layer. Although we are primarily interested in the release of gases from the lower layer, it is of interest to estimate the growth rate of the Rayleigh-Taylor instability, $1/\beta$, should sufficient methane be added to result in $\rho_1 < \rho_2$. The result depends strongly on the density difference $\rho_2 - \rho_1$. Using (4.23) and the values of the parameters in (4.15) but with $\rho_1 = 999.9\,\mathrm{kg\ m^{-3}}$ and $\rho_1 = 999\,\mathrm{kg\ m^{-3}}$ we obtain

$$\frac{1}{\beta} = 6.43\,\mathrm{hrs} \qquad \text{and} \qquad \frac{1}{\beta} = 2.03\,\mathrm{hrs}\ , \tag{4.24}$$

respectively.

The fast and slow internal waves on the picnocline generate fast and slow waves on the surface of the lake given by

$$\eta_2(x,t) = -\frac{p_A}{g\,\rho_2} + \left[\frac{\rho_1}{\rho_2}\ \frac{(h_1+h_2)}{2h_1}\left\{1 \pm \left(1 - \frac{4(\rho_1-\rho_2)}{\rho_1}\ \frac{h_1h_2}{(h_1+h_2)^2}\right)^{1/2}\right\} - \frac{(\rho_1-\rho_2)}{\rho_2}\right]\ \eta_{10}\exp\left[i(kx-\omega t)\right] \tag{4.25}$$

which have the same speed and frequency as the internal waves but have a different amplitude. Equation (4.25) is derived in Apendix A as equation (A.79). Expanding

(4.25), neglecting terms of order δ^2 and taking the real part we obtain for the fast surface wave

$$\eta_2(x,t) \; + \; \frac{p_A}{g\,\rho_2}$$

$$= \; \frac{(h_1+h_2)}{h_1} \; \left[1 + \frac{(\rho_1-\rho_2)}{\rho_2} \, \frac{h_2^2}{(h_1+h_2)^2}\right] \eta_{10} \cos\left[k(x-c_+t)\right] \qquad (4.26)$$

and for the slow surface wave

$$\eta_2(x,t) + \frac{p_A}{g\,\rho_2} = -\frac{(\rho_1-\rho_2)}{\rho_2} \, \frac{h_1}{(h_1+h_2)} \, \eta_{10} \; \cos\left[k(x-c_-t)\right] \, . \qquad (4.27)$$

Using the values of the physical quantities in (4.15) we obtain for the fast surface wave

$$\eta_2(x,t) + \frac{p_B}{g\,\rho_2} = 2.155\left[1 + 2.8 \times 10^{-4}\right] \, \eta_{20} \; \cos\left[k(x-c_+t)\right] \qquad (4.28)$$

and for the slow surface wave

$$\eta_2(x,t) + \frac{p_B}{g\,\rho_2} = -4.64 \times 10^{-4} \, \eta_{10} \; \cos\left[k(x-c_-t)\right] \, . \qquad (4.29)$$

The fast surface wave will be stable for all positive values of ρ_1 and ρ_2 but the slow surface wave will be unstable if $\rho_2 > \rho_1$ with characteristic growth time $1/\beta$ where β is given by (4.23).

The amplitude of the fast wave on the surface is greater than the amplitude η_{10} of the internal waves at the picnocline by a factor of $(h_1+h_2)/h_1$. An internal wave of amplitude $\eta_{10} = 2\,\mathrm{m}$ might be expected from a minor volcanic eruption and would give rise to a fast wave on the surface of amplitude 4.3 m which could cause damage around the shores of the lake. The slow surface wave has a phase difference of π with the slow internal wave. Its amplitude is proportional to $\rho_1 - \rho_2$ and is negligibly small when the density difference across the picnocline is small. The fast wave is more dangerous than the slow wave at the surface of the lake because of its greater amplitude and speed, but at the picnocline the slow wave is much more dangerous than the fast wave because it allows more time for gases to escape from the fluid.

The pressure changes associated with the internal wave at the interface could cause gas bubbles to form if the sum of the partial pressures of the carbon dioxide and the methane approach the local hydrostatic pressure and the water approaches supersaturation conditions. The fast and slow internal pressure waves on the picnocline are given by

$p_1(x,0,t) = p_2(x,0,t)$

$$= \rho_2\, g\, h_2$$
$$+\rho_1\, g \left[\frac{(h_1+h_2)}{2h_1} \left\{ 1 \pm \left(1 - \frac{4(\rho_1-\rho_2)}{\rho_1} \, \frac{h_1\, h_2}{(h_1+h_2)^2} \right)^{1/2} \right\} - 1 \right] \eta_{10} \exp\left[i(kx-\omega t) \right] . \tag{4.30}$$

Equation (4.30) is derived in Appendix A as (A.80). Expanding (4.30) neglecting terms of order δ^2 and taking the real part gives for the fast pressure wave

$$p_1(x,0,t) - \rho_2\, g\, h_2 = \rho_1\, g\, \frac{h_2}{h_1} \left[1 - \frac{(\rho_1-\rho_2)}{\rho_1} \, \frac{h_1}{(h_1+h_2)} \right] \eta_{10} \, \cos\left[k(x-c_+t) \right] \tag{4.31}$$

and for the slow pressure wave

$$p_1(x,0,t) - \rho_2\, g\, h_2 = -\rho_1\, g \left[1 - \frac{(\rho_1-\rho_2)}{\rho_1} \, \frac{h_2}{(h_1+h_2)} \right] \eta_{10} \, \cos\left[k(x-c_-t) \right] . \tag{4.32}$$

For the values of the physical quantities given in (4.15) and expressed in Pascals, the fast pressure wave is

$$p_1(x,0,t) - 2.55 \times 10^6 = 1.13 \times 10^4 \left[1 - 4.63 \times 10^{-4} \right] \eta_{10} \, \cos\left[k(x-c_+t) \right] , \tag{4.33}$$

and the slow pressure wave is

$$p_1(x,0,t) - 2.55 \times 10^6 = -9.82 \times 10^3 \left[1 - 5.36 \times 10^{-4} \right] \eta_{10} \, \cos\left[k(x-c_-t) \right] . \tag{4.34}$$

Although the ratio of the pressure change in the slow wave to that in the fast wave is approximately $h_1/h_2 = 0.865$ the slow wave plays a more important part in the formation of bubbles because the larger period of the slow wave, about sixty times greater than the period of the fast wave, gives more time for the formation of bubbles. For the slow wave the maximum displacement corresponds to the minimum pressure. This is expected because the wave will lift the fluid to a higher level. Interestingly, for the fast wave the opposite is the case and the maximum displacement corresponds to the maximum pressure.

The amplitude of the fast pressure wave is approximately

$$\rho_1\, g\, \frac{h_2}{h_1} \, \eta_{10} = 1.13 \times 10^4 \text{ Pa} \tag{4.35}$$

for $\eta_{10} = 2\,\text{m}$ which could be expected for a minor eruption. The hydrostatic pressure at 260 m is

$$\rho_2\, g\, h_2 = 2.55 \times 10^6 \text{ Pa} . \tag{4.36}$$

The ratio of the maximum pressure change in the fast wave to the hydrostatic pressure at the picnocline is therefore

$$\frac{\rho_1}{\rho_2} \, \frac{\eta_{10}}{h_1} = 8.8 \times 10^{-3} = 0.88\% . \tag{4.37}$$

For the slow pressure wave, its amplitude is

$$\rho_1 \, g \, \eta_{10} = 9.82 \times 10^3 \, \mathrm{Pa} \tag{4.38}$$

and the ratio of this pressure to the hydrostatic pressure at the picnocline is

$$\frac{\rho_1}{\rho_2} \, \frac{\eta_{10}}{h_2} = 7.7 \times 10^{-3} = 0.77\% \; . \tag{4.39}$$

These pressure changes will only likely affect the number of heterogeneous nucleation sites unless the water is supersaturated in which case all the gases at the interface will be spontaneously released.

Finally, consider the path of a fluid particle in the lower layers due to the internal wave on the interface [7]. A fluid particle is initially at $x = X_0$, $y = Y_0$. At a later time

$$x = X_0 + X_1(t) \; , \qquad y = Y_0 + Y_1(t) \; , \tag{4.40}$$

where

$$X_1(0) = 0 \; , \qquad Y_1(0) = 0 \tag{4.41}$$

and

$$\frac{\mathrm{d}X_1}{\mathrm{d}t} = \frac{\partial \phi_1}{\partial x} = v_x^{(1)}(x, y, t) \; , \tag{4.42}$$

$$\frac{\mathrm{d}Y_1}{\mathrm{d}t} = \frac{\partial \phi_1}{\partial y} = v_x^{(1)}(x, y, t) \; . \tag{4.43}$$

We use (A.85) and (A.86) derived in Appendix A for $v_x^{(1)}(x, y, t)$ and $v_y^{(1)}(x, y, t)$. Thus

$$v_x^{(1)}(x, y, t) = \omega \eta_{10} \left[\frac{1}{k \, h_1} + \left(\frac{1}{3} + \frac{y}{h_1} + \frac{1}{2} \, \left(\frac{y}{h_1} \right)^2 \right) k \, h_1 \right.$$

$$\left. + \mathrm{O}\Big((k \, h_1)^3 \Big) \right] \cos(kx - \omega t \quad) \; , \tag{4.44}$$

$$v_y^{(1)}(x, y, t) = \omega \eta_{10} \left[1 + \frac{y}{h_1} + \left(\frac{1}{3} \, \frac{y}{h_1} + \frac{1}{2} \, \left(\frac{y}{h_1} \right)^2 + \frac{1}{6} \left(\frac{y}{h_1} \right)^3 \right) (k \, h_1)^2 \right.$$

$$\left. + \mathrm{O}\Big((k \, h_1)^4 \Big) \right] \sin(kx - \omega t) \; , \tag{4.45}$$

and make the approximation of replacing x and y by X_0 and Y_0.Then

$$\frac{\mathrm{d}X_1}{\mathrm{d}t} = \frac{\omega\eta_{10}}{k\,h_1}\left[1+\mathrm{O}\big((k\,h_1)^2\big)\right]\,\cos(k\,X_0-\omega t)\;, \tag{4.46}$$

$$\frac{\mathrm{d}Y_1}{\mathrm{d}t} = \omega\eta_{10}\,\left[1+\frac{Y_0}{h_1}+\mathrm{O}\big((k\,h_1)^2\big)\right]\,\sin(k\,X_0-\omega t)\;. \tag{4.47}$$

Integrating with respect to time and imposing the initial conditions (4.41) gives

$$X_1(t) = -\frac{\eta_{10}}{k\,h_1}\Big[1+\mathrm{O}\big((k\,h_1)^2\big)\Big]\,\sin(k\,X_0-\omega t)+\alpha\;, \tag{4.48}$$

$$Y_1(t) = +\eta_{10}\left[1+\frac{Y_0}{h_1}+\mathrm{O}\big((k\,h_1)^2\big)\right]\cos(k\,X_0-\omega t)+\beta\;, \tag{4.49}$$

where

$$\alpha = \frac{\eta_{10}}{k\,h_1}\Big[1+\mathrm{O}\big((k\,h_1)^2\big)\Big]\,\sin(k\,X_0)\;, \tag{4.50}$$

$$\beta = -\eta_{10}\left[1+\frac{Y_0}{h_1}+\mathrm{O}\big((k\,h_1)^2\big)\right]\cos(k\,X_0)\;. \tag{4.51}$$

Substituting (4.48) and (4.49) into (4.40) and eliminating time t we obtain

$$\frac{\big(x-(X_0+\alpha)\big)^2}{A^2}+\frac{\big(y-(Y_0+\beta)\big)^2}{B^2}=1\;, \tag{4.52}$$

where

$$A = \frac{\eta_{10}}{k\,h_1}\Big(1+\mathrm{O}\big((k\,h_1)^2\big)\Big)\;, \tag{4.53}$$

$$B = \eta_{10}\left(1+\frac{Y_0}{h_1}+\mathrm{O}\big((k\,h_1)^2\big)\right)\;. \tag{4.54}$$

The particle path is therefore an ellipse with centre at $(X_0+\alpha,\ Y_0+\beta)$ and semi-major axis A and semi-minor axis B.

A fluid particle describes the ellipse clockwise when the wave is propagating in the positive x-direction and a fluid particle on a crest moves in the direction of the wave and in a trough it moves in the opposite direction to the wave.

The fluid particle describes the ellipse with the same period as the wave that generates the motion. Although the particle path is the same for both the fast and slow waves a significant difference in the particle motion driven by the fast and slow wave is the time it takes for the particle to move round the ellipse. These times are given by (4.13) and(4.14) for the fast and slow waves. For the values of the physical parameters given in (4.15) it takes 12.08 min for a particle to describe the ellipse driven by the fast wave and 12.78 hrs to describe the ellipse driven by the slow wave which is 63 times

longer. There is therefore more time for the bubbles to form in the part of the orbit with reduced pressure when the motion is driven by the slow wave.

For both the fast and slow waves the semi-major and semi-minor axes of the ellipse are given by (4.53) and (4.54). Using the values given by (4.15) and an internal wave amplitude $\eta_{10} = 2\,\mathrm{m}$,

$$A = 70.77\Big[1 + \mathrm{O}\left(8 \times 10^{-4}\right)\Big]\mathrm{m}\ , \tag{4.55}$$

$$B = 2\left[1 + \frac{Y_0}{h_1} + \mathrm{O}\left(8 \times 10^{-4}\right)\right]\mathrm{m}\ , \quad -225 \leq Y_0 \leq 0\ . \tag{4.56}$$

The eccentricity of the ellipse at $Y_0 = 0$ is $\mathrm{e} = 0.9996$. The semi-major axis decreases very slowly with depth. More important for the formation of bubbles in the lower layer is the steady decrease in the semi-minor axis with depth. At the bottom of the lake, $Y_0 = -h_1 = -225\,\mathrm{m}$, and $B = 0$ thus satisfying the boundary condition

$$y = -h_1 : \qquad \frac{\partial \phi_1}{\partial y}\left(x, -h_1, t\right) = 0\ . \tag{4.57}$$

on the normal component of the fluid velocity which was imposed through (A.27) on the solution in Appendix A. The fluid particles slip on the bed of the lake and oscillate horizontally with no pressure change.

The results of this section show that two internal waves can propagate on the picnocline, a fast wave and a slow wave. Although the pressure change due to the slow wave is slightly less than that of the fast wave the slow wave is much more important in the formation of bubbles. The period of the slow wave is about sixty times greater than that of the fast wave which gives much more time for bubble formation. However, the pressure changes due to the internal waves are very small and will only be important if the water is supersaturated. The fast and slow internal waves on the picnocline generate fast and slow waves with the same speed and frequency on the surface of the lake. The amplitude of the slow wave on the surface is proportional to the density difference across the picnocline and is very small but the amplitude of the fast wave is more than twice the amplitude of the fast wave on the interface and could cause damage around the shores of the lake. On the surface of the lake the fast wave is more dangerous than the slow wave because of its greater amplitude and speed and this is independent of whether or not degassing occurs. The fluid particle path in the lower layer due to the internal wave on the interface describes an ellipse with the same period as the wave which generates the motion. The particle path is the same for both the slow and fast wave but the particle takes about sixty times longer to describe the ellipse driven by the slow wave which gives more time to form bubbles. The semi-minor axis of the ellipse decreases steadily with depth and therefore the formation of bubbles in the lower layer due to the internal wave on the interface will decrease steadily with depth.

5 Siphoning off the gas: a chimney model

Gas can be extracted from the lake by extending a pipe from the surface into the lower layer containing the gas. Because of stratification the siphon will extract liquid from a lake wide horizontal layer at the same level as that of the lower end of the pipe. Eventually liquid will be drained from above that level but not from below so the pipe end should be as deep as possible whilst covering as much lake area as possible. The siphon needs to be primed by first sucking fluid up the pipe. A pressure gradient will develop along the pipe, and fluid particles travelling up the pipe will be subjected to a lower pressure than those outside the pipe and absorbed gases will be released. The buoyancy uplift will then act to carry the fluid particles up and out the siphon, as seen in Figure 15. The methane then needs to be separated out from the carbon dioxide and sent to the power station. There are several flow regimes that can occur in the siphon

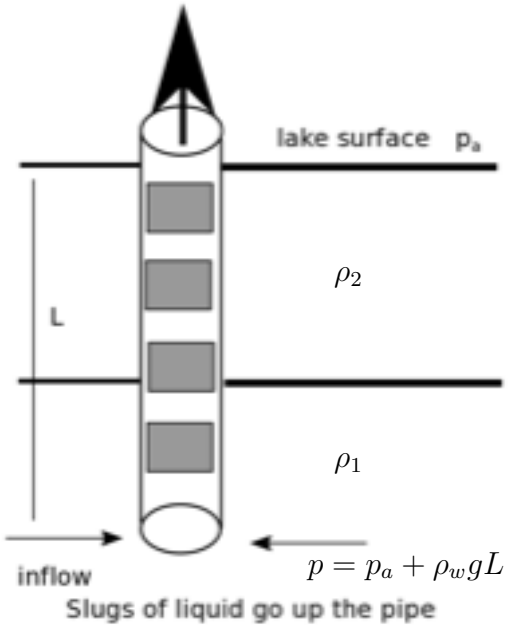

Figure 19: The chimney model.

pipe depending on the bubble/liquid volume ratio, but we will assume 'plug flow', see Wallis [11]. It could well be that there are engineering advantages in arranging for the flow to be restricted to one of the flow types by changing the radius of the pipe or the length of the pipe; we will address such issues here.

Gas flows up the chimney/pipe length L because the density ρ_p inside the pipe is less than the density ρ_w outside the chimney/pipe.

5.1 The chimney model

The pressure drop driving the flow is given by $(\rho_w - \rho_p)gL$ where ρ_w is the water density outside the pipe, ρ_p the (average) mass per unit volume (of water and gas) inside the pipe. Bernoulli's principle determines the flow velocity v of the gas and water mixture going up the pipe as

$$(\rho_w - \rho_p)gL = \frac{1}{2}\rho_w v^2 \ ,$$

assuming gas and water move with the same velocity v, so

$$v = \sqrt{\frac{2(\rho_w - \rho_p)gL}{\rho_w}} \ .$$

The associated volume flux of water is approximately given by

$$\sqrt{\frac{2(\rho_w - \rho_p)gL}{\rho_w}} A \ ,$$

where A is the pipe area; the mass flux of gas is relatively small. The gas flux out of the pipe is obtained by factoring in the gas concentration at the bottom end of the pipe.

Note that the pipe flux increases in proportion to the square root of density difference between the outside and inside of the pipe times the pipe length.

6 Conclusions

Based on the data and observations presented in The Report on Lake Stability [1] we have examined the processes of gas accumulation and release in Lake Kivu. Because of the high pressure levels in the lower stratification layers gas will be stored until saturation levels are reached and observations suggest this would first occur at the top of the lowest stratification layer. A more detailed hydrodynamic model would be required to understand what determines the observed stratification, however present observations indicate that the present layering is not changing with time. Any such change, which could be caused by 'natural processes' or human intervention (extracting methane), would be extremely significant.

We examined the generation of internal waves within the lake due to eruptions; such eruptions can cause gas release. The results indicate that both fast (periods about 12 mins) and slow travelling waves (periods of about 12 hours) will be generated

by ground movements associated with eruptions. Because of long period and relatively large amplitude of the slow internal wave, gas is more likely to be released by these slow waves. Thus one would expect eruption induced 'vibrations' with periods of about 12 hours to be most damaging as far as gas release is concerned. Thus for example mud slides on the bottom of the lake are likely to be more dangerous than higher frequency impulse vibrations. Gas release is likely to occur near the edge of the lake because of the nonlinear build up of the wave height.

Whilst we can claim to understand the mechanisms involved in this release, it is difficult to obtain estimates for the volume of gas release under specific eruption circumstances because the amplitude and modal mix of the internal waves generated by an eruption will strongly depend on the specifics of the ground movement. Thus for example a vertical displacement of the lake's bottom will generate a large slow internal wave which will result in large gas release, whereas a horizontal movement of the bottom will generate no internal wave with no gas release (as with a tsunami). Additionally there is much uncertainty associated with bubble production. The bubbles will be produced by heterogeneous nucleation and the number of nucleation sites will depend on conditions above the lake as well as below its surface. For example if there is a wind blowing then dust particles in air falling on the lake will sink and act as nucleation sites; under eruption conditions weather patterns are probably unpredictable. An overestimate of the gas release can be obtained by assuming that all gas will be released from the pycnocline zone with the zone thickness related to the amplitude of the slow wave generated by a prescribed vertical drop on the lake's bottom; this calculation is under way.

Acknowledgments

In conclusion we would like to say that this was a very interesting and important problem brought to us by Denis Ndanguza who actively participated; thank you. The problem attracted about thirty enthusiastic participants that addressed many different issues. The attendance level was such that it was impossible to include all in the list of Study Group participants but do know that your contributions were much appreciated and needed. The work done was excellent! Much remains to be done but we made a start.

References

[1] Kling G W, MacIntyre S, Steenfelt J S and Hirslund F. Lake Kivu gas extraction-Report on lake stability. Report to the World Bank (2006).

[2] Ross K A, Gashugi E, Gafasi A, Wüest A and Schmid M. Characterisation of the subaquatic groundwater discharge that maintains the permanent stratification within Lake Kivu; East Africa. PlOS one 10.3 (2015): e0121217.

[3] Tietze K. The Lake Kivu methane - problem of extraction and their mathematical-physical study. Regional Conference on Petroleum Industry and Manpower Requirements in the Field of Hydrocarbons, 2–12 February, 1974, Tripoli, Lybya. United Nations Economic and Social Council, United Nations Economic Commission for Africa, E/CN, 14/INF/13, Tripoli, 5 December 1973, 7p.

[4] Schmid M, Tietze K, Halbwachs M, Lorke A, McGinnis D and Wŭest A. How hazardous is the gas accumulation in Lake Kivu? Arguments for a risk assesment in light of the Nyiragongo volcanic eruption of 2002. Acta Vulcanologica, **15** (2003), 115-122.

[5] Schmid M, Halbwachs M, Wehrli B and Wüst A. Weak mixing in Lake Kivu: new insights indicate increasing risk of uncontrolled gas eruption. Geochemistry, Geophysics, Geosystems **6**, (2005), 1–11.

[6] Schmid M, Kelly K A and Wüest A. Comment on An additional challenge of Lake Kivu in Central Africa-upward movement of the chemoclines by Finn Hirslund. Journal of Limnology **71**, (2012), e35.

[7] Billingham J and King A C. Wave Motion, Cambridge University Press, Cambridge 2006, pp 81-82.

[8] Acheson D J. Elementary Fluid Dynamics, Clarendon Press, Oxford, 1990, pp 8-10.

[9] Batchelor G K. An Introduction to Fluid Dynamics, Cambridge University Press, Cambridge, 1967.

[10] Witherspoon PA and Saraf D N. Diffusion of methane, ethane, propane and n-butane in water from 25 to 43°. Journal of Physical Chemistry, **69**, (1965), 3752–3755.

[11] Wallis G B. One-dimensional two-phase flow. McGraw-Hill, New York, 1970.

Appendix

A Internal waves

Four layers have been identified in Lake Kivu. When considering internal layers the three upper layers are combined to form one uniform layer from the surface of the lake to a depth of 260 m. The fourth and lowest layer which contains the dissolved methane and carbon dioxide has a thickness of 225 m and extends from a depth of 260 m to the bottom of the lake at 485 m. The interface between the two layers is called the picnocline. In this Appendix we present the mathematical formulation and mathematical solution for internal waves on the picnocline. The results are analysed in Section 4.

Internal waves may be generated by volcanic activity or by a seismic event. Mud slides could also generate an internal wave. The wavelength of the internal wave will be the order of magnitude of the length or width of the lake. The maximum width is 48 km. The wavelength will therefore be greater than about 50 km and therefore much greater than the depth of the lake. The amplitude of the wave will be much smaller than the depth and therefore the approximations of shallow water waves can be made. Boundary conditions will be imposed at the bottom of the lake and at the surface.

A diagram of the lake and the coordinate system is presented in Figure 18. The origin of the coordinate system is on the picnocline with the x-axis along the picnocline and the y-axis vertically upwards. The bottom of the lake is at $y = -h_1 = -225\,\mathrm{m}$ and the surface is at $y = h_2 = 260\,\mathrm{m}$. Suffices 1 and 2 will be used to denote fluid variables in the lower and upper fluids, respectively.

A.1 Mathematical formulation

The internal wave generated on the picnocline is

$$y = \eta_1(x,t) \tag{A.1}$$

and this will generate at the surface of the lake the wave

$$y = h_2 + \eta_2\,(x,t)\ . \tag{A.2}$$

It is assumed that both fluids are inviscid and incompressible with densities ρ_1 and ρ_2. Thus

$$\boldsymbol{\nabla}\cdot\boldsymbol{v}^{(1)} = 0, \qquad \boldsymbol{\nabla}\cdot\boldsymbol{v}^{(2)} = 0\ , \tag{A.3}$$

where $\boldsymbol{v}$ denotes the fluid velocity. It is also assumed that both fluids are irrotational so that

$$\boldsymbol{\omega}^{(1)} = \boldsymbol{\nabla}\times\boldsymbol{v}^{(1)} = \mathbf{0}\ , \qquad \boldsymbol{\omega}^{(2)} = \boldsymbol{\nabla}\times\boldsymbol{v}^{(2)} = \mathbf{0}\ . \tag{A.4}$$

Thus

$$\boldsymbol{v}^{(1)} = \boldsymbol{\nabla}\phi_1 \ , \qquad \boldsymbol{v}^{(2)} = \boldsymbol{\nabla}\phi_2 \ , \tag{A.5}$$

where $\phi = \phi(x, y, t)$ is the velocity potential. From (A.3) and (A.5) the velocity potential satisfies Laplace's equation,

$$\nabla^2\phi_1 = 0 \ , \qquad \nabla^2\phi_2 = 0 \ . \tag{A.6}$$

We make the approximation that the amplitudes of the waves are sufficiently small that the squares and products of ϕ_1 , ϕ_2 , η_1 , η_2 and their partial derivatives can be neglected.

We now impose the interface and boundary conditions.

(i) Fluid velocity at the interface $y = \eta_1(x, t)$

A fluid particle on the interface remains on the interface as the fluid evolves. Thus

$$\frac{\mathrm{D}}{\mathrm{D}t}\left(y - \eta_1(x,t)\right)\bigg|_{y=\eta_1(x,t)} = 0 \ , \tag{A.7}$$

where $\frac{\mathrm{D}}{\mathrm{D}t}$ denotes the convective time derivative. Thus

$$v_y(x, \eta_1, t) = \frac{\partial \eta_1}{\partial t}\ (x,t) + v_x(x, \eta_1, t)\ \frac{\partial \eta_1}{\partial x} \ . \tag{A.8}$$

We perform a Taylor expansion about $y = 0$ and neglect second order terms in smallness. This is equivalent to imposing the interface condition on $y = 0$. Thus

$$y = 0 : \qquad v_y(x, 0, t) = \frac{\partial \eta_1}{\partial t}(x,t) \tag{A.9}$$

and since (A.9)applies for a fluid particle from both the lower and upper fluid the following two interface conditions are obtained:

$$y = 0 : \qquad \frac{\partial \phi_1}{\partial y}\ (x, 0, t) = \frac{\partial \eta_1}{\partial t}\ (x,t) \ , \tag{A.10}$$

$$y = 0 : \qquad \frac{\partial \phi_2}{\partial y}\ (x, 0, t) = \frac{\partial \eta_1}{\partial t}\ (x,t) \ . \tag{A.11}$$

(ii) Fluid pressure at the interface $y = \eta_1(x, t)$

The normal stresses must balance at the interface. Since the viscosity is zero in both fluids the only normal stress in the pressure. Bernoulli's equation for the unsteady irrotational inviscid flow under gravity in each layer is [8]

$$\frac{\partial \phi_n}{\partial t} + \frac{1}{2}\left[\left(\frac{\partial \phi_n}{\partial x}\right)^2 + \left(\frac{\partial \phi_n}{\partial y}\right)^2\right] + \frac{p}{\rho_n} + g\, y = G_n(t) \ , \quad n = 1, 2, \tag{A.12}$$

where $p = p\,(x, y, t)$ is the fluid pressure and $G(t)$ is an arbitrary function which has to be determined.

Consider first the upper fluid. For the fluid at rest and at $y = 0$, $\phi_2(x, 0, t) = 0$ and $p_2(x, 0, t) = \rho_2\, g\, h_2$. Thus

$$G(t) = g\, h_2 \tag{A.13}$$

and (A.12) with second order terms neglected becomes

$$\frac{\partial \phi_2}{\partial t}\,(x, y, t) + \frac{1}{\rho_2}\Big(p_2(x, y, t) - \rho_2\, g\, h_2\Big) + g\, y = 0\,. \tag{A.14}$$

Thus

$$p_2(x, y, t) - \rho_2\, g\, h_2 = -\rho_2\,\left[\frac{\partial \phi_2}{\partial t}\,(x, y, t) + g\, y\right]\,. \tag{A.15}$$

Consider next the lower fluid. For the fluid at rest and at $y = 0$, $\phi_1(x, 0, t) = 0$, $p_1(x, 0, t) = \rho_2\, g\, h_2$ and therefore

$$G_1(t) = \frac{\rho_2}{\rho_1}\, g\, h_2\,. \tag{A.16}$$

Equation (A.12) with second order terms neglected becomes

$$\frac{\partial \phi_1}{\partial t}\,(x, y, t) + \frac{1}{\rho_1}\Big(p_1(x, y, t) - \rho_2\, g\, h_2\Big) + g\, y = 0\,, \tag{A.17}$$

which gives

$$p_1(x, y, t) - \rho_2\, g\, h_2 = -\rho_1\,\left[\frac{\partial \phi_1}{\partial t}\,(x, y, t) + g\, y\right]\,. \tag{A.18}$$

Since the normal stress must balance at the interface,

$$y = \eta(x, t): \qquad p_1(x, \eta_1, t) = p_2\,(x, \eta_1, t)\,. \tag{A.19}$$

We use (A.15) and (A.18) and expand about $y = 0$ neglecting second order terms. This gives the interfacial condition

$$y = 0: \qquad \rho_1\left[\frac{\partial \phi_1}{\partial t}\,(x, 0, t) + g\,\eta_1\,(x, t)\right] = \rho_2\,\left[\frac{\partial \phi_2}{\partial t}\,(x, 0, t) + g\,\eta_1\,(x, t)\right]\,. \tag{A.20}$$

(iii) Fluid velocity at the interface $y = h_2 + \eta_2\,(x, t)$

A fluid particle on the surface of the lake remains on the surface as the fluid evolves. Thus

$$\frac{\mathrm{D}}{\mathrm{D}t}\Big(y - \big(h_2 + \eta_2\,(x, t)\big)\Big)\Big|_{y = h_2 + \eta_2(x,t)} = 0 \tag{A.21}$$

and hence

$$v_y(x, h_2 + \eta_2, t) = \frac{\partial}{\partial t}\,\eta_2\,(x,t) + v_x\,(x, h_2 + \eta_2, t)\,\frac{\partial \eta_2}{\partial x}\,(x,t)\;. \tag{A.22}$$

By expanding about $y = h_2$ and neglecting second order terms we obtain

$$y = h_2: \qquad \frac{\partial \phi_2}{\partial y}\,(x, h_2, t) = \frac{\partial \eta_2}{\partial t}\,(x,t)\;. \tag{A.23}$$

(iv) Fluid pressure at the interface $y = h_2 + \eta_2\,(x,t)$

Since the normal stresses must balance at the surface of the lake,

$$y = h_2 + \eta_2\,(x,t): \qquad p_2(x, h_2 + \eta_2, t) = p_A\;, \tag{A.24}$$

where p_A is the atmospheric pressure. Using (A.15) for $p_2(x,y,t)$, equation (A.24) becomes

$$y = h_2 + \eta_2(x,t): \qquad -\rho_2\left[\frac{\partial \phi_2}{\partial t}\,(x, h_2 + \eta_2, t) + g\,\eta_2\,(x,t)\right] = p_A \tag{A.25}$$

and expanding about $y = h_2$ and neglecting second order terms we obtain the interface condition

$$y = h_2: \qquad \frac{\partial \phi_2}{\partial t}\,(x, h_2, t) + g\,\eta_2\,(x,t) = -\frac{p_A}{\rho_2}\;. \tag{A.26}$$

(v) Boundary condition at $y = -h_1$

The normal component of the fluid velocity must vanish at the bottom of the lake. Hence

$$y = -h_1: \qquad \frac{\partial \phi_1}{\partial y}\,(x, -h_1, t) = 0\;. \tag{A.27}$$

The problem can be summarised as follows.
Solve for $\eta_1(x,t),\ \eta_2(x,t),\ \phi_1(x,y,t)$ and $\phi_2(x,y,t)$ the Laplace equations

$$\frac{\partial^2 \phi_1}{\partial x^2} + \frac{\partial^2 \phi_1}{\partial y^2} = 0\;, \tag{A.28}$$

$$\frac{\partial^2 \phi_2}{\partial x^2} + \frac{\partial^2 \phi_2}{\partial y^2} = 0\;, \tag{A.29}$$

subject to the interface and boundary conditions

$$y = 0: \quad \frac{\partial \phi_1}{\partial y}(x,0,t) = \frac{\partial \eta_1}{\partial t}(x,t), \tag{A.30}$$

$$y = 0: \quad \frac{\partial \phi_2}{\partial y}(x,0,t) = \frac{\partial \eta_1}{\partial t}(x,t), \tag{A.31}$$

$$y = 0: \quad \rho_1 \left[\frac{\partial \phi_1}{\partial t}(x,0,t) + g\,\eta_1(x,t)\right] = \rho_2 \left[\frac{\partial \phi_2}{\partial t}(x,0,t) + g\,\eta_1(x,t)\right], \tag{A.32}$$

$$y = h_2: \quad \frac{\partial \phi_2}{\partial y}(x,h_2,t) = \frac{\partial \eta_2}{\partial t}(x,t), \tag{A.33}$$

$$y = h_2: \quad \frac{\partial \phi_2}{\partial y}(x,h_2,t) + g\,\eta_2(x,t) = -\frac{p_A}{\rho_2}, \tag{A.34}$$

$$y = -h_1: \ \frac{\partial \phi_1}{\partial y}(x,-h_1,t) = 0. \tag{A.35}$$

Once the problem has been solved the pressure at the interface $y = 0$ is given by

$$p_1(x,0,t) = \rho_2\, g\, h_2 - \rho_1 \left[\frac{\partial \phi_1}{\partial t}(x,0,t) + g\,\eta_1(x,t)\right] \tag{A.36}$$

or equivalently, since $p_1(x,0,t) = p_2(x,0,t)$, by

$$p_2(x,0,t) = \rho_2\, g\, h_2 - \rho_2 \left[\frac{\partial \phi_2}{\partial t}(x,0,t) + g\,\eta_1(x,t)\right]. \tag{A.37}$$

A.2 Mathematical solution

We first eliminate $\eta_1(x,t)$ and $\eta_2(x,t)$ from the interface and boundary conditions. From (A.32) and (A.34),

$$\eta_1(x,t) = -\frac{1}{(\rho_1 - \rho_2)\, g}\left[\rho_2 \frac{\partial \phi_2}{\partial t}(x,0,t) - \rho_1 \frac{\partial \phi_1}{\partial t}(x,0,t)\right], \tag{A.38}$$

$$\eta_2(x,t) = -\frac{1}{g}\left[\frac{p_A}{\rho_2} + \frac{\partial \phi_2}{\partial t}(x,h_2,t)\right]. \tag{A.39}$$

Using (A.38) and (A.39), equations (A.30), (A.31), (A.33) and (A.35) become

$$y = 0: \qquad \frac{\partial \phi_1}{\partial y}(x,0,t) + \frac{1}{(\rho_1 - \rho_2)\, g}\left[\rho_1 \frac{\partial^2 \phi_1}{\partial t^2}(x,0,t) - \rho_2 \frac{\partial^2 \phi_2}{\partial t^2}(x,0,t)\right] = 0\,, \tag{A.40}$$

$$y = 0: \quad \frac{\partial \phi_2}{\partial y}(x,0,t) + \frac{1}{(\rho_1 - \rho_2)\, g}\left[\rho_1 \frac{\partial^2 \phi_1}{\partial t^2}(x,0,t) - \rho_2 \frac{\partial^2 \phi_2}{\partial t^2}(x,0,t)\right] = 0\ , \quad \text{(A.41)}$$

$$y = h_2: \quad \frac{\partial \phi_2}{\partial y}(x,h_2,t) + \frac{1}{g}\frac{\partial^2 \phi_2}{\partial t^2}(x,h_2,t) = 0\ , \quad \text{(A.42)}$$

$$y = -h_1: \quad \frac{\partial \phi_1}{\partial y}(x,-h_1,t) = 0\ . \quad \text{(A.43)}$$

The problem has now been expressed in terms of $\phi_1(x,y,t)$ and $\phi_2(x,y,t)$ alone. It consists in solving the partial differential equations (A.28) and (A.29) for $\phi_1(x,y,t)$ and $\phi_2(x,y,t)$ subject to the four conditions, (A.40) to (A.43). Once $\phi_1(x,y,t)$ and $\phi_2(x,y,t)$ have been determined, the internal wave $\eta_1(x,t)$ and the surface wave $\eta_2(x,t)$ are obtained from (A.38) and (A.39) and the fluid pressure at the interface $y = 0$ is obtained from (A.36) or equivalently (A.37).

We look for solutions of the form

$$\phi_n(x,y,t) = F_n(y) \exp\left[i(kx - \omega t)\right], \qquad n = 1,2 \quad \text{(A.44)}$$

and at the end of the calculation the real part is taken. In (A.44)

$$k = \frac{2\pi}{\lambda}\ , \qquad \omega = \frac{2\pi}{T}\ , \qquad \frac{\omega}{k} = c\ , \quad \text{(A.45)}$$

where k is the wave number λ the wave length, ω the angular frequency, T the period and c the phase velocity of the wave. Complex values of ω/k are interpreted as instabilities of the interface.

Substituting (A.44) into (A.28) and (A.29) gives

$$\frac{\mathrm{d}^2 F_n}{\mathrm{d}y^2} - k^2 F_n = 0\ , \qquad n = 1,2 \quad \text{(A.46)}$$

and therefore

$$F_n(y) = A_n \cosh(ky) + B_n \sinh(ky) \quad \text{(A.47)}$$

where A_n and B_n are constants. Thus

$$\phi_n(x,y,t) = \left[A_n \cosh(ky) + B_n \sinh(ky)\right] \exp\left[i(kx - \omega t)\right], \quad n = 1,2\ . \quad \text{(A.48)}$$

The four constants A_1, B_1 A_2 and B_2 are obtained form the four interface and boundary conditions, (A.40) to (A.43). Substituting (A.48) into (A.40) to (A.43) gives the four homogeneous algebraic equations

$$\frac{\rho_1}{(\rho_1 - \rho_2)}\frac{\omega^2}{k} A_1 \quad - g\, B_1 \qquad\qquad - \frac{\rho_2}{(\rho_1 - \rho_2)}\frac{\omega^2}{k} A_2 \qquad\qquad = 0, \quad \text{(A.49)}$$

$$\frac{\rho_1}{(\rho_1 - \rho_2)}\frac{\omega^2}{k} A_1 \qquad\qquad - \frac{\rho_2}{(\rho_1 - \rho_2)}\frac{\omega^2}{k} A_2 \quad - g\, B_2 \quad = 0, \quad \text{(A.50)}$$

$$\sinh(k\,h_1)\, A_1 \qquad - \cosh(k\,h_1)\, B_1 \qquad\qquad\qquad\qquad = 0, \quad \text{(A.51)}$$

$$\left[\frac{\omega^2}{k}\,\cosh(k\,h_2) - g\,\sinh(k\,h_2)\right]\,A_2 + \left[\frac{\omega^2}{k}\,\sinh(k\,h_2) - g\,\cosh(k\,h_2)\right]\,B_2 = 0\;. \tag{A.52}$$

Equations (A.49) to (A.52) can be written in matrix form as

$$GX = 0 \tag{A.53}$$

where

$$G = \begin{bmatrix} \dfrac{\rho_1}{(\rho_1-\rho_2)}\,\dfrac{\omega^2}{k} & -g & -\dfrac{\rho_2}{(\rho_1-\rho_2)}\,\dfrac{\omega^2}{k} & 0 \\ \dfrac{\rho_1}{(\rho_1-\rho_2)}\,\dfrac{\omega^2}{k} & 0 & -\dfrac{\rho_2}{(\rho_1-\rho_2)}\,\dfrac{\omega^2}{k} & -g \\ \sinh(kh_1) & -\cosh(kh_1) & 0 & 0 \\ 0 & 0 & \dfrac{\omega^2}{k}\,\cosh(kh_2) & \dfrac{\omega^2}{k}\,\sinh(kh_2) \\ & & -g\,\sinh(kh_2) & -g\,\cosh(kh_2) \end{bmatrix} \tag{A.54}$$

and

$$X = \begin{bmatrix} A_1 & B_1 & A_2 & B_2 \end{bmatrix}^T\;. \tag{A.55}$$

Equation (A.54) has a nontrivial solution for X provided

$$\det\,[G] = 0\;, \tag{A.56}$$

that is, provided,

$$\Big[\rho_2\sinh(k\,h_1)\sinh(k\,h_2) + \rho_1\cosh(k\,h_1)\,\cosh(k\,h_2)\Big]\,\frac{\omega^4}{k^2} - g\,\rho_1\sinh\Big(k(h_1+h_2)\Big)\,\frac{\omega^2}{k} + g^2\,\big(\rho_1-\rho_2\big)\,\sinh\,(k\,h_1)\sinh\,(k\,h_2) = 0\;. \tag{A.57}$$

Equation (A.57) is the dispersion equation for the internal waves at the interface $y = 0$ and for the waves at the surface $y = h_2$.

Equation(A.57) is valid for all wavelengths. Consider waves of long wavelength and an expansion in powers of $k\,h$. Now

$$\sinh x = \sum_{n=0}^{\infty}\,\frac{x^{2n+1}}{(2n+1)!} = x + \frac{x^3}{6} + \mathrm{O}(x^5)\;, \tag{A.58}$$

$$\cosh x = \sum_{n=0}^{\infty} \frac{x^{2n}}{(2n)!} = 1 + \frac{x^2}{2} + \mathrm{O}(x^4) \;, \tag{A.59}$$

as $x \to 0$. Expanding (A.57) in powers of $k\,h_1$, $k\,h_2$ and $k\,(h_1+h_2)$ we obtain

$$\left[\rho_1 + \frac{1}{2}\,\rho_1\,(k\,h_1)^2 + \frac{1}{2}\,\rho_1\,(k\,h_2)^2 + \rho_2\,k\,h_1\;k\,h_2 + \mathrm{O}\Big((k\,h)^4\Big)\right]\;\frac{\omega^4}{k^2}$$

$$-\rho_1 g\left[k\,(h_1+h_2) + \mathrm{O}\Big((k\,h)^3\Big)\right]\;\frac{\omega^2}{k} + (\rho_1-\rho_2)g^2\left[k\,h_1\;k\,h_2 + \mathrm{O}\Big((k\,h)^4\Big)\right] = 0\;. \tag{A.60}$$

Correct to first order in $k\,h$ the dispersion equation (A.60) is

$$\rho_1\;\frac{\omega^2}{k}\;\left[\frac{\omega^2}{k} - k(h_1+h_2)\,g\right] = 0 \tag{A.61}$$

and therefore

$$c = \frac{\omega}{k} = 0\;, \qquad c = \frac{\omega}{k} = \pm\Big[(h_1+h_2)\,g\Big]^{1/2}\;. \tag{A.62}$$

Correct to second order in $k\,h$ the dispersion equation (A.60) is

$$\left[\rho_1 + \frac{1}{2}\,\rho_1\,(k\,h_1)^2 + \frac{1}{2}\,\rho_1\,(k\,h_2)^2 + \rho_2\,k\,h_1\;k\,h_2\right]\;\frac{\omega^4}{h^2}$$

$$-\rho_1\,g\,k\,(h_1+h_2)\;\frac{\omega^2}{k} + (\rho_1-\rho_2)\,g^2\,k\,h_1\;k\,h_2 = 0\;. \tag{A.63}$$

Solving the quadratic equation (A.63) for ω^2/k and neglecting terms $\mathrm{O}\big((k\,h)^3\big)$ we obtain

$$c = \frac{\omega}{k} = \pm\left[\frac{g}{2}\left(h_1+h_2 \pm \left[(h_1+h_2)^2 - \frac{4(\rho_1-\rho_2)}{\rho_1}\;h_1\,h_2\right]^{1/2}\right)\right]^{1/2} \tag{A.64}$$

which can be written equivalently as

$$c = \frac{\omega}{k} = \pm\left[\frac{g}{2}\left(h_1+h_2 \pm \left[(h_1-h_2)^2 + 4\frac{\rho_2}{\rho_1}\;h_1\,h_2\right]^{1/2}\right)\right]^{1/2}\;. \tag{A.65}$$

This dispersion equation will be analysed in the next subsection.

By using (A.48) for $\phi_1(x,0,t)$, $\phi_2(x,0,t)$ and $\phi_2(x,h_2,t)$ we can express (A.38), (A.39) and (A.36), or equivalently (A.37), in terms of the constants A_1, B_1, A_2 and B_2 as

$$\eta_1(x,t) \;= \frac{i\omega}{(\rho_1-\rho_2)\,g}\;(\rho_1\,A_1 - \rho_2\,A_2)\exp\;\Big[i(kx-\omega t)\Big]\;, \tag{A.66}$$

$$\eta_2(x,t) \ = -\frac{p_A}{g\,\rho_2} + \frac{i\,\omega}{g}\,\Big[A_2\cosh(k\,h_2) + B_2\sinh(k\,h_2)\Big]\exp\Big[i(kx-\omega t)\Big]\,, \qquad \text{(A.67)}$$

$$p_1(x,0,t) = p_2(x,0,t)$$

$$= \rho_2\,g\,h_2 + i\,\omega\,\frac{\rho_1\,\rho_2}{(\rho_1-\rho_2)}\,(A_2-A_1)\,\exp\,\Big[i(kx-\omega t)\Big]\,. \qquad \text{(A.68)}$$

Because (A.53) is an eigenvalue problem only three of the four constants $A_1,\ B_1,\ A_2,\ B_2$ and only three of the four equations (A.49) to (A.52) are independent. We can only solve for any three of $A_1,\ B_1,\ A_2$ and B_2 in terms of a fourth. We use equations (A.49) to (A.51) to solve for $A_1,\ A_2,\ B_2$ in terms of B_1. It can be verified that

$$A_1 = \coth\,(k\,h_1)\,B_1\,, \qquad \text{(A.69)}$$

$$A_2 = \left[\frac{\rho_1}{\rho_2}\,\coth\,(k\,h_1) - g\,\frac{(\rho_1-\rho_2)}{\rho_2}\,\frac{k}{\omega^2}\right]\,B_1\,, \qquad \text{(A.70)}$$

$$B_2 = B_1\,. \qquad \text{(A.71)}$$

Equation (A.66) becomes

$$\eta_1\,(x,t) = \frac{i\,k}{\omega}\,B_1\,\exp\,\Big[i(kx-\omega t)\Big]\,. \qquad \text{(A.72)}$$

But

$$\eta_1\,(x,t) = \eta_{10}\,\exp\,\Big[i(kx-\omega t)\Big] \qquad \text{(A.73)}$$

where the constant η_{10} is the prescribed amplitude of the wave at the interface. Hence

$$B_1 = \frac{\omega}{i\,k}\,\eta_{10} \qquad \text{(A.74)}$$

and $A_1,\ A_2$ and B_2 can be expressed in terms of η_{10} instead of B_1. Equations (A.67) and (A.68) become

$$\eta_2(x,t) = -\frac{p_A}{g\,\rho_2} + \frac{1}{g}\,\left[\frac{\omega^2}{k}\,\frac{\cosh\,\big(k(h_1+h_2)\big)}{\sinh\,(k\,h_1)}\right.$$

$$\left. +\frac{(\rho_1-\rho_2)}{\rho_2}\,\cosh\,(k\,h_2)\left\{\frac{\omega^2}{k}\,\coth\,(k\,h_1) - g\right\}\right]\,\eta_{10}\exp\,\Big[i(kx-\omega t)\Big]\,, \qquad \text{(A.75)}$$

$$p_1(x,0,t) = p_2(x,0,t)$$

$$= \rho_2\,g\,h_2 + \rho_1\,\left[\frac{\omega^2}{k}\,\coth\,(k\,h_1) - g\right]\,\eta_{10}\,\exp\,\Big[i(kx-\omega t)\Big]\,, \qquad \text{(A.76)}$$

where ω^3/k satisfies the quadratic equation(A.57).

Equation (A.75 and (A.76) apply for all wavelengths. Consider waves of long wavelength and make an expansion in powers of $k\,h$. We use expansions (A.58) and (A.59) for $\sinh x$ and $\cosh x$ and the expansion

$$\coth x = \frac{1}{x} + \frac{1}{3}\,x + \mathrm{O}(x^3) \quad \text{as} \quad x \to 0\ . \tag{A.77}$$

Also from (A.64),

$$\frac{\omega^2}{k} = \frac{g}{2}\,k(h_1+h_2)\,\left[1 \pm \left(1 - \frac{4(\rho_1-\rho_2)}{\rho_1}\,\frac{h_1\,h_2}{(h_1+h_2)}\right)^{1/2}\right] + \mathrm{O}\big((k\,h)^2\big)\ . \tag{A.78}$$

Equations (A.75) and (A.76) become

$$\eta_2(x,t) = -\frac{p_A}{g\,\rho_2} + \left[\frac{\rho_1}{\rho_2}\,\frac{(h_1+h_2)}{2h_1}\left\{1 \pm \left(1 - \frac{4(\rho_1-\rho_2)}{\rho_1}\,\frac{h_1 h_2}{(h_1+h_2)^2}\right)^{1/2}\right\} - \frac{(\rho_1-\rho_2)}{\rho_2}\right]\,\eta_{10}\exp\big[i(kx-\omega t)\big] \tag{A.79}$$

and

$$\begin{aligned} p_1(x,0,t) &= p_2(x,0,t) \\ &= \rho_2\,g\,h_2 \\ &+\rho_1\,g\left[\frac{(h_1+h_2)}{2h_1}\left\{1 \pm \left(1 - \frac{4(\rho_1-\rho_2)}{\rho_1}\,\frac{h_1\,h_2}{(h_1+h_2)^2}\right)^{1/2}\right\} - 1\right]\eta_{10}\exp\big[i(kx-\omega t)\big] \end{aligned} \tag{A.80}$$

where terms of order $(k\,h)^2$ are neglected. Equations (A.79) and (A.80) will be considered further in Section 4.

In Section 4 we will investigate the paths of the fluid particles in the lower layer as the wave propagates on the interface. To do that we will require the $x-$ and $y-$ components of the fluid velocity in the lower layer. Now, from (A.48) and using (A.69) and (A.74),

$$\phi_1(x,y,t) = -\frac{i\omega}{k}\,\eta_{10}\Big[\coth(k\,h_1)\cosh(ky) + \sinh(ky)\Big]\exp\big[i(kx-\omega t)\big] \tag{A.81}$$

and taking the real part gives

$$\phi_1(x,y,t) = \frac{\omega}{k}\,\eta_{10}\Big[\coth(h\,h_1)\cosh(ky) + \sinh(ky)\Big]\sin(kx-\omega t)\ . \tag{A.82}$$

Hence

$$v_x^{(1)}(x,y,t) = \frac{\partial \phi_1}{\partial x}$$

$$= \omega\,\eta_{10}\Big[\coth(k\,h_1)\cosh(ky) + \sinh(ky)\Big]\cos(kx-\omega t) \tag{A.83}$$

and

$$v_y^{(1)}(x,y,t) = \frac{\partial \phi_1}{\partial y}$$

$$= \omega\,\eta_{10}\Big[\coth(k\,h_1)\sinh(ky) + \cosh(ky)\Big]\sin(kx-\omega t)\ . \tag{A.84}$$

Expanding (A.83) and (A.84) in powers of $k\,h_1$ and ky for long wavelengths using (A.58), (A.59) and (A.77) gives

$$v_x^{(1)}(x,y,t) = \omega\eta_{10}\left[\frac{1}{k\,h_1} + \left(\frac{1}{3} + \frac{y}{h_1} + \frac{1}{2}\,\left(\frac{y}{h_1}\right)^2\right)k\,h_1 \right.$$

$$\left. + \mathrm{O}\Big((k\,h_1)^3\Big)\right]\cos(kx-\omega t)\ , \tag{A.85}$$

$$v_y^{(1)}(x,y,t) = \omega\eta_{10}\left[1 + \frac{y}{h_1} + \left(\frac{1}{3}\,\frac{y}{h_1} + \frac{1}{2}\,\left(\frac{y}{h_1}\right)^2 + \frac{1}{6}\left(\frac{y}{h_1}\right)^3\right)(k\,h_1)^2 \right.$$

$$\left. + \mathrm{O}\Big((k\,h_1)^4\Big)\right]\sin(kx-\omega t)\ , \tag{A.86}$$

where ω/k is given by (A.64).

This completes the mathematical solution. The results are analysed in Section 4.